

000
001  **CATCH: CHANNEL-AWARE MULTIVARIATE TIME**
002 **SERIES ANOMALY DETECTION VIA FREQUENCY**
003 **PATCHING**
004
005
006
007
008 **Anonymous authors**
009 Paper under double-blind review
010
011
012

ABSTRACT

013 Anomaly detection in multivariate time series is challenging as heterogeneous
014 subsequence anomalies may occur. Reconstruction-based methods, which focus
015 on learning normal patterns in the frequency domain to detect diverse abnormal
016 subsequences, achieve promising results, while still falling short on capturing fine-
017 grained frequency characteristics and channel correlations. To contend with the
018 limitations, we introduce CATCH, a framework based on frequency patching. We
019 propose to patchify the frequency domain into frequency bands, which enhances
020 its ability to capture fine-grained frequency characteristics. To perceive appro-
021 priate channel correlations, we propose a Channel Fusion Module (CFM), which
022 features a patch-wise mask generator and a masked-attention mechanism. Driven
023 by a bi-level multi-objective optimization algorithm, the CFM is encouraged to
024 iteratively discover appropriate patch-wise channel correlations, and to cluster rel-
025 evant channels while isolating adverse effects from irrelevant channels. Extensive
026 experiments on 9 real-world datasets and 12 synthetic datasets demonstrate that
027 CATCH achieves state-of-the-art performance. We make our code and datasets
028 available at <https://anonymous.4open.science/r/CATCH-E535>.
029
030 **1 INTRODUCTION**
031

032 Modern cyber physical systems are often monitored by multiple sensors, which produce successive
033 multivariate time series data. Multivariate Time Series Anomaly Detection (MTSAD) aims to detect
034 abnormal data in multivariate time series. It is applied widely including but not limited to financial
035 fraud detection, medical disease identification, and cybersecurity threat detection (Li et al., 2021;
036 Wen et al., 2022; Yang et al., 2023a; Kieu et al., 2018; 2019).

037 Time series anomalies are typically classified into point anomalies and subsequence anomalies. The
038 point anomalies can be further classified as *contextual* or *global* anomalies (Lai et al., 2021). Re-
039 cent reconstruction-based methods show strong capability of detecting point anomalies, which are
040 characterized by specific values that significantly deviate from the normal range of the probability
041 distribution. However, subsequence anomalies consist of values that fall within the probability dis-
042 tribution, making them much harder to detect (Paparrizos et al., 2022b; Nam et al., 2024). According
043 to the behavior-driven taxonomy (Lai et al., 2021), the subsequence anomalies can be further divided
044 into *seasonal*, *shapelet*, and *trend* anomalies—see Figure 1a. A promising approach is to transform
045 the time series into the frequency domain to better derive the subsequence anomalies.

046 When transformed into the frequency domain, distinct subsequence anomalies also show promi-
047 nent differences against the normal series in different frequency bands (Figure 1a). In this case,
048 shapelet anomalies mainly affect the third frequency band while seasonal anomalies affect the
049 first two frequency bands. However, the frequency domain features a long-tailed distribution
050 that most information centralizes in the low frequency bands. Coarse-grained reconstruc-
051 tion-based methods may neglect the details in the high frequency bands (Guo et al., 2023; Piao
052 et al., 2024; Park & Kim, 2022; Wang et al., 2022), thus failing to detect correspond anomalies,
053 which calls for *fine-grained modeling in each frequency band* to precisely reconstruct the nor-
 mal patterns, so that heterogeneous subsequence anomalies can be detected. Moreover, consider-
 ing the relationships among channels also promotes better reconstruction for normal patterns.

Figure 1b shows a multivariate time series with three channels, and we observe the varying channel associations in different frequency bands, where Channel 1 and Channel 2 are similar in the third band but dissimilar to Channel 3, and all channels are similar in the fourth band but show dissimilarity in the fifth. However, the commonly-used Channel-Independent (CI) and Channel-Dependent (CD) strategies exhibit polarization effects, rendering them inadequate for this task. CI uses the same model across different channels and overlooks potential channel correlations, which offers robustness (Nie et al., 2023) but lacks generalizability and capacity. CD considers all channels simultaneously with larger capacity, but may be susceptible to noise from irrelevant channels, thus lacking robustness (Han et al., 2024). This calls for *flexibly adapting the distinct channel interrelationships in different frequency bands*.

Inspired by the above observations, we propose **CATCH**, a Channel-Aware MTSAD framework via frequency patching. Technically, we utilize Fourier Transformation to stretch across time and frequency domains to facilitate the detection of both point and subsequence anomalies, of which the latter can be improved by patching in the frequency domain for fine-grained modeling. To flexibly utilize the channel correlations in frequency bands, we propose a Channel Fusion Module (CFM) that incorporates a Channel Correlation Discovering mechanism and utilizes masked attention through a bi-level multi-objective optimization process. Specifically, we utilize a patch-wise mask generator to adaptively discover channel correlation for each frequency band. The discovered channel correlation is between CI and CD, providing both the capacity and robustness by clustering relevant channels while isolating the adverse effects from irrelevant channels. The contributions are summarized as follows:

- We propose a general framework called CATCH, which enables simultaneous detection of heterogeneous point and subsequence anomalies via frequency patch learning. The framework enhances subsequence anomaly detection through frequency-domain patching and integrates fine-grained adaptive channel correlations across frequency bands.
- We design the CFM to fully utilize the fine-grained channel correlations. Driven by a bi-level multi-objective optimization algorithm, the CFM is able to iteratively discover appropriate channel correlations and facilitate the isolation of irrelevant channels and the clustering of relevant channels, which provides both the capacity and robustness.
- We conduct extensive experiments on 21 multivariate datasets. The results show that CATCH outperforms state-of-the-art baselines.

2 RELATED WORK

2.1 MULTIVARIATE TIME-SERIES ANOMALY DETECTION

Traditional MTSAD methods can be classified into non-learning (Breunig et al., 2000; Goldstein & Dengel, 2012; Yeh et al., 2016) and machine learning (Liu et al., 2008; Ramaswamy et al., 2000).

108 Recently, deep learning methods have shown exceptional MTSAD performance and have received
 109 substantial extensive attention. They can be classified into forecasting-based, reconstruction-based
 110 and contrastive-based methods. GDN (Deng & Hooi, 2021) is a forecasting-based model that uses a
 111 graph structure to learn topology and a graph attention network to encode input series, with anomaly
 112 detection based on the maximum forecast error among channel variables. Anomaly Transformer is a
 113 reconstructive approach that combines series and prior association to make anomalies distinctive (Xu
 114 et al., 2021). DCdetector uses contrastive learning in anomaly detection to create an embedding
 115 space where normal data samples are close together and anomalies are farther apart (Yang et al.,
 116 2023b). We focus on the reconstruction-based methods due to their prominent performance on
 117 commonly-used benchmark datasets (Qiu et al., 2024).

118

119

120 2.2 CHANNEL STRATEGIES IN MTSAD

121

122 A channel refers to a variable in MTSAD, while a channel strategy refers to how these channel cor-
 123 relations are effectively considered during the modeling process. CATCH employs a reconstruction-
 124 based anomaly detection algorithm, using reconstruction error as the anomaly score, making re-
 125 construction quality crucial for anomaly detection accuracy. Since the channels in multivariate
 126 time series often exhibit complex dependencies, explicitly modeling these correlations enables a
 127 more comprehensive capture of global features, thereby improving reconstruction capabilities and
 128 anomaly detection performance. There are mainly two existing approaches that consider relation-
 129 ships among channels. Channel-Independent (CI) based methods such as: PatchTST (Nie et al.,
 130 2023) and DLinear (Zeng et al., 2023) impose the constraint of using the same model across differ-
 131 ent channels. While it offers robustness, it overlooks potential interactions among channels and can
 132 be limited in generalizability and capacity for unseen channels (Han et al., 2024). Previous studies
 133 have shown that correlation discovery in data is crucial for time series anomaly detection (Song
 134 et al., 2018). Channel-Dependent (CD) based methods such as: MSCRED (Zhang et al., 2019) uses
 135 a convolutional-LSTM network with attention and a loss function to reconstruct correlation mat-
 136 rices among channels in multivariate time series input. iTransformer (Liu et al., 2024) embeds time
 137 points into variate tokens and applies an attention mechanism to capture multivariate correlations.
 138 MTAD-GAT (Zhao et al., 2020) treats each univariate time series as a feature and uses two parallel
 139 graph attention layers to capture dependencies across both temporal and channel dimensions. The
 140 existing methods could not adequately extract interrelationships, they may be susceptible to noise
 141 from irrelevant channels, reducing the model’s robustness.

142

143

144 2.3 FREQUENCY DOMAIN ANALYSIS FOR TSAD

145

146

147

148

149

150

151

152

153

154

155

156

157

158

159

160

161

Frequency domain analysis can uncover subsequence anomalies that are challenging to detect
 in the time domain, such as anomalies in periodic fluctuations or oscillation patterns, signif-
 icantly enhancing detection accuracy (Zhang et al., 2022). Consequently, frequency-based
 time series anomaly detection models have garnered widespread attention in recent years.

Table 1: Comparison of existing frequency-based
 TSAD methods.

Property	Multivariate time serie anomaly detection	Time-frequency granularity alignment	Handle high-frequency information	Capture channel correlations
SR-CNN	✗	✗	✗	✗
PFT	✗	✗	✗	✗
TFAD	✓	✗	✗	✗
Dual-TF	✓	✓	✗	✗
CATCH	✓	✓	✓	✓

SR-CNN (Ren et al., 2019), the first method to leverage the frequency domain for TSAD, em-
 ploys a frequency-based approach to generate saliency maps for identifying anomalies, and
 PFT (Zhang et al., 2022) built on this founda-
 tion by introducing partial Fourier transform to
 achieve substantial acceleration. However, both
 methods are confined to univariate time series and fail to address the complexities of multivariate
 scenarios. TFAD (Nam et al., 2024) emerges as the first approach to integrate time-domain and
 frequency-domain analyses for MTSAD, yet it lacks time-frequency granularity alignment. Dual-
 TF (Nam et al., 2024), the most recent algorithm for MTSAD using time-frequency analysis, par-
 tially addresses the time-frequency granularity alignment issue but lacks a tailored backbone, instead
 relying directly on the Anomaly Transformer (Xu et al., 2021). While TFAD and Dual-TF repre-
 sent progress in this area, they still exhibit the following limitations: i) Frequency-domain modeling
 methods have inherent biases, often overlooking high-frequency information; 2) Insufficient explo-
 ration and utilization of channel correlations in multivariate time series.

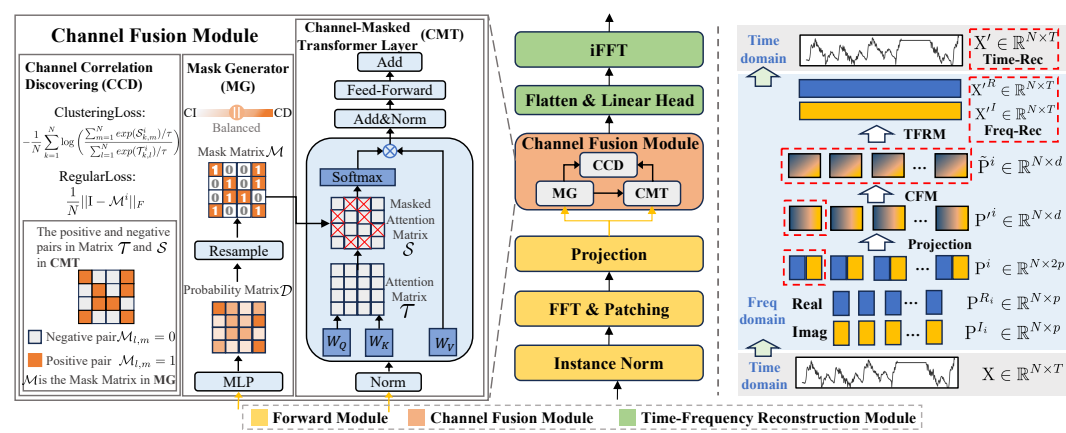


Figure 2: **CATCH** architecture. (1) Forward Module normalizes the input data, patchifies the frequency domain, and then projects it into the hidden space. (2) Channel Fusion Module captures channel interrelationships in each frequency band with a Channel-Masked Transformer (CMT) Layer, where the mask matrix (channel correlation) is generated by Mask Generator (MG). During training, MG and CMT are optimized by Channel Correlation Discovering (CCD) for more appropriate channel correlations. (3) Time-Frequency Reconstruction Module obtains the frequency reconstruction through Flatten & Linear Head Layer, and obtains the time reconstruction after iFFT.

3 CATCH

In the context of time series anomaly detection, $X \in \mathbb{R}^{N \times T}$ denotes a time series with N channels and length T . For clear delineation, we separate dimensions with commas and use this format throughout this paper. For example, we denote $X_{i,j}$ as the i -th channel at the j -th timestamp, $X_{n,:} \in \mathbb{R}^T$ as the time series of n -th channel, where $n = 1, 2, \dots, N$. The multivariate time series anomaly detection problem is to determine whether $X_{:,t}$ is anomaly or not.

3.1 STRUCTURE OVERVIEW

Figure 2 shows the overall architecture of the **CATCH**, which consists of three main **modules**: 1) the **Forward Module**, 2) the **Channel Fusion Module** (CFM), and 3) the **Time-Frequency Reconstruction Module** (TFRM). Specifically, the input multivariate time series is firstly processed via the **Forward Module**, consisting of the **Instance Norm Layer**, **FFT&Patching Layer**, and **Projection Layer**.

The **Instance Norm Layer** is firstly to mitigate the distributional shifts between the training and testing data caused by varying statistical properties, enhancing the model’s generalization in reconstructing the testing data. Then, the **FFT&Patching Layer** is to perform fine-grained modeling in each frequency band (patch). Specifically, we utilize the efficient FFT (Brigham & Morrow, 1967) to transform time series into orthogonal trigonometric signals in the frequency domain, where we keep both the real and imaginary parts through $X^R, X^I = \text{FFT}(X)$ for maximum information retention, where $X, X^R, X^I \in \mathbb{R}^{N \times T}$. Next, we apply the frequency patching operation to create fine-grained frequency bands (patches), which can be formalized as follows.

$$\{P^{R_1}, P^{R_2}, \dots, P^{R_L}\} = \text{Patching}(X^R), \{P^{I_1}, P^{I_2}, \dots, P^{I_L}\} = \text{Patching}(X^I), \quad (1)$$

where $P^{R_i}, P^{I_i} \in \mathbb{R}^{N \times p}$ denote the i -th patch of X^R and X^I . $L = [T - p]/s + 1$ is the total patch number, where p is the patch size and s is the patch stride.

We then concat each pair of P^{R_i} and P^{I_i} into $P^i \in \mathbb{R}^{N \times 2p}$, as the i -th frequency patch. After patching in the frequency domain, the frequency patches are then projected into the high-dimensional hidden space through the **Projection Layer**: $P'^i = \text{Projection}(P^i)$.

After the **Forward Module**, the processed time series is fed into the **Channel Fusion Module** (CFM) to dynamically model the channel correlations in each fine-grained frequency band.

$$\{\tilde{P}^1, \tilde{P}^2, \dots, \tilde{P}^L\} = \text{CFM}(\{P'^1, P'^2, \dots, P'^L\}), \quad (2)$$

216 where $P'^i, \tilde{P}^i \in \mathbb{R}^{N \times d}$, N is the number of channels and d is the hidden dimension in attention
 217 blocks. The CFM parallels in a patch-wise way to model the frequency patches simultaneously. We
 218 further introduce the details of CFM in Section 3.2.

219 Next, we utilize the *Time-Frequency Reconstruction Module* (TFRM) to reconstruct all frequency
 220 spectrums for real and imaginary patches and simultaneously obtain their temporal reconstruction:
 221

$$222 \quad X', X'^R, X'^I = \text{TFRM}(\{\tilde{P}^{R_1}, \tilde{P}^{R_2}, \dots, \tilde{P}^{R_L}\}, \{\tilde{P}^{I_1}, \tilde{P}^{I_2}, \dots, \tilde{P}^{I_L}\}), \quad (3)$$

223 where X' is the temporal reconstruction, and $X'^R, X'^I \in \mathbb{R}^{N \times T}$ are the frequency reconstruction.
 224 Finally, we integrate the reconstruction error in both time and frequency domains as anomaly score.
 225

226 3.2 CHANNEL FUSION MODULE

228 The *Channel Fusion Module* (CFM) contains the following three components: 1) the *Mask Generator*
 229 (MG), 2) the *Channel-Masked Transformer Layer* (CMT), and 3) the *Channel Correlation*
 230 *Discovering* (CCD) mechanism. Specifically, the MG is to perceive and generate the mask matrices
 231 (channel correlations) in different frequency bands and guide the masked attention in CMT. The
 232 CMT aims to model the appropriate patch-wise channel correlations. And the CCD is to guide the
 233 MG and CMT to explore better channel correlations during optimization.

234 **Mask Generator.** Inspired by Selective State Space Models such as Mamba (Gu & Dao, 2023;
 235 Dao & Gu, 2024), which utilizes Linear projections to flexibly update the hidden states based on the
 236 current data for larger capacity, the patch-wise channel associations can also be treated as a changing
 237 hidden state strongly associated with the current patch. Therefore, we devise a Linear-based mask
 238 generator to perceive the suitable channel associations for each frequency band by generating binary
 239 mask matrices to isolate the adverse effects from irrelevant channels. Note that the binary mask is
 240 an intermediate state between CI (identity matrix) and CD (all-ones matrix) strategies. Moreover,
 241 the *Mask Generator* itself works in a CI manner to mitigate the adverse effects from noisy channels.
 242 We take the i -th frequency patch as an example:

$$243 \quad D^i = \sigma(\text{Linear}(P'^i)), \mathcal{M}^i = \text{Resample}(D^i), \quad (4)$$

245 where $P'^i \in \mathbb{R}^{N \times d}$, $D^i \in \mathbb{R}^{N \times N}$, and $\mathcal{M}^i \in \mathbb{R}^{N \times N}$ are the hidden representation, the probability
 246 matrix, and the binary mask matrix of i -th patch, respectively. σ projects the values to probabilities.

247 Since our goal is to filter out the adverse effects of irrelevant channels, we further perform Bernoulli
 248 resampling on the probability matrices to obtain binary mask matrix \mathcal{M}^i with the same shape.
 249 Higher probability $D_{l,m}^i$ results in $\mathcal{M}_{l,m}^i$ closer to 1, indicating a relationship between channel l
 250 and channel m . And we manually keep the diagonal items to 1. To ensure the propagation of
 251 gradients, we use the Gumbel Softmax reparameterization trick (Jang et al., 2017) during Bernoulli
 252 resampling.

253 **Channel-Masked Transformer Layer.** After the *Mask Generator* outputs the mask matrices for
 254 frequency bands, we utilize the transformer layer to further capture the fine-grained channel corre-
 255 lations. The Layer Normalization is applied before each attention block to mitigate the over-focusing
 256 phenomenon on frequency components with larger amplitudes (Piao et al., 2024):

$$257 \quad P^{*i} = \text{LayerNorm}(P'^i) = (P'^i - \text{Mean}_{n=1}^N(P'^i_{n,:})) / \sqrt{\text{Var}_{n=1}^N(P'^i_{n,:})}, \quad (5)$$

259 where $P'^i \in \mathbb{R}^{N \times d}$ and $P^{*i} \in \mathbb{R}^{N \times d}$ are the hidden representation and the normalized representa-
 260 tion of i -th patch, respectively. Empirically, we utilize the masked attention mechanism to further
 261 model the fine-grained interrelationships among relevant channels and integrate the mask matrix in
 262 a calculated way to keep the propagation of gradients:

$$263 \quad Q^i = P^{*i} \cdot W^Q, K^i = P^{*i} \cdot W^K, V^i = P^{*i} \cdot W^V, \quad (6)$$

$$265 \quad \mathcal{T}^i = Q^i \cdot (K^i)^T, \mathcal{S}^i = \mathcal{T}^i \odot \mathcal{M}^i + (1 - \mathcal{M}^i) \odot (-\infty), \quad (7)$$

$$266 \quad \text{MaskedScores}^i = \mathcal{S}^i / \sqrt{d}, \tilde{P}^i = \text{Softmax}(\text{MaskedScores}^i) \cdot V^i, \quad (8)$$

268 where $W^Q, W^K, W^V \in \mathbb{R}^{d \times d}$, $\mathcal{M}^i \in \mathbb{R}^{N \times N}$, $\mathcal{T}^i \in \mathbb{R}^{N \times N}$, $\mathcal{S}^i \in \mathbb{R}^{N \times N}$, and $\tilde{P}^i \in \mathbb{R}^{N \times d}$ are the
 269 binary mask matrix, the attention matrix, the masked attention matrix, and the hidden representation
 processed by CMT of i -th patch, respectively.

We utilize the same Feed-Forward networks and skip connections as the classical transformers (Vaswani, 2017). We also apply multi-head mechanism to jointly attend to information from different representational subspaces and the CMT can be stacked multiple times.

Channel Correlation Discovering. From an optimization perspective, it is essential to design appropriate optimization objectives to enhance the effectiveness of generated masks. A direct motivation is to explicitly enhance the attention scores between relevant channels defined by the mask, thus aligning the attention mechanism with the currently discovered optimal channel correlation, which helps isolate the adverse effects from irrelevant channels and provides robustness for the attention mechanism. Then we iteratively optimize the *Mask Generator* to refine the channel correlations, tuning the capacity of attention mechanism in the *Channel-Masked Transformer Layer* to fully capture the interrelationships between channels. Intuitively, we devise two loss functions to guide the *Mask Generator* exploring the space of channel correlations (from CI to CD). The proposed loss functions are formalized as:

$$\text{ClusteringLoss} = -\frac{1}{N} \sum_{k=1}^N \log \left(\frac{\sum_{m=1}^N \exp(\mathcal{S}_{k,m}^i)/\tau}{\sum_{l=1}^N \exp(\mathcal{T}_{k,l}^i)/\tau} \right), \quad (9) \quad \text{RegularLoss} = \frac{1}{N} \|\mathbf{I} - \mathcal{M}^i\|_F, \quad (10)$$

where τ is the temperature coefficient, N is the number of channels, \mathbf{I} is the identity matrix, and $\|\cdot\|_F$ is the Frobenius norm. $\mathcal{T}^i \in \mathbb{R}^{N \times N}$, $\mathcal{S}^i \in \mathbb{R}^{N \times N}$, and $\mathcal{M}^i \in \mathbb{R}^{N \times N}$ are the attention matrix, the masked attention matrix, and the binary mask matrix for i -th patch, respectively.

The ClusteringLoss is similar to the InfoNCE (He et al., 2020) in form but does not fix the number of “positive” pairs. In contrast, it changes its “positive” pairs for different patches based on the current discovered channel correlation \mathcal{M}^i . Theoretically, the similarities between “positive” or “negative” pairs are also calculated through inner product, so we share the calculating results of \mathcal{S}^i and \mathcal{T}^i from the attention mechanism to save the computational cost. As shown in Figure 2, we exhibit the “positive” and “negative” pairs in the attention matrix \mathcal{T} and masked attention matrix \mathcal{S} . Specifically, it sets the Query and Key views of relevant channels in a frequency band ($\mathcal{M}_{l,m}^i = 1$) as the “positive” pairs, otherwise ($\mathcal{M}_{l,m}^i = 0$) “negative” pairs, thus encouraging the \mathbf{W}^Q and \mathbf{W}^K to cluster the patch-wise relevant channels in the hidden spaces and lead to higher attention scores. However, only a single ClusteringLoss may cause some adverse effects by urging the *Mask Generator* to output constant ones matrix, so that we add a RegularLoss to mitigate this risk by restricting the number of relevant channels. Equipped with the two optimization objectives, the *Mask Generator* is encouraged to discover appropriate patch-wise channel correlations between CI and CD, and the attention mechanism is also enhanced by optimizing the \mathbf{W}^Q and \mathbf{W}^K to learn fine-grained channel representations in the hidden spaces.

3.3 TIME FREQUENCY RECONSTRUCTION MODULE

The *Time-Frequency Reconstruction Module* (TFRM) contains the following two components: 1) the *Flatten & Linear Head Layer* and 2) the *iFFT Layer*. Specifically, after the CFM fully extract the fine-grained channel correlations, we utilize the TFRM to flatten the patch-wise representations and reconstruct all frequency spectrums with MLP projections separately for real and imaginary patches, and obtain temporal reconstruction through iFFT:

$$\mathbf{X}'^R = \text{Projection}_R(\text{FlattenHead}(\{\tilde{\mathbf{P}}^{R_1}, \tilde{\mathbf{P}}^{R_2}, \dots, \tilde{\mathbf{P}}^{R_L}\})), \quad (11)$$

$$\mathbf{X}'^I = \text{Projection}_I(\text{FlattenHead}(\{\tilde{\mathbf{P}}^{I_1}, \tilde{\mathbf{P}}^{I_2}, \dots, \tilde{\mathbf{P}}^{I_L}\})), \quad (12)$$

$$\mathbf{X}' = \text{iFFT}(\mathbf{X}'^R, \mathbf{X}'^I) \quad (13)$$

where \mathbf{X}'^R , \mathbf{X}'^I , and $\mathbf{X}' \in \mathbb{R}^{N \times T}$. We then adopt the reconstruction loss functions both in time and frequency domains to separately enhance the ability of point-to-point and sequence modeling. The reconstruction functions in time and frequency domains are formalized as:

$$\text{RecLoss}^{time} = \|\mathbf{X} - \mathbf{X}'\|_F^2 \quad (14) \quad \text{RecLoss}^{freq} = \|\mathbf{X}^R - \mathbf{X}'^R\|_1 + \|\mathbf{X}^I - \mathbf{X}'^I\|_1 \quad (15)$$

We utilize 2-norm in the time domain and 1-norm in the frequency domain due to the distinct numerical characteristics of time and frequency domains (Wang et al., 2024).

324 3.4 JOINT BI-LEVEL OPTIMIZATION
325

326 We then design a novel joint bi-level training process to enhance the model’s ability to detect both
327 point anomalies and subsequence anomalies. Our TotalLoss \mathcal{L} mainly consists of reconstruction
328 loss functions in the time ($\text{RecLoss}^{\text{time}}$) and frequency ($\text{RecLoss}^{\text{freq}}$) domains, ClusteringLoss
329 and RegularLoss from the *Channel Correlation Discovering* mechanism. The reconstruction loss
330 functions are used to enhance model’s ability in both time and frequency domains to detect point
331 and subsequence anomalies. The ClusteringLoss and RegularLoss are used to guide the discovering
332 for fine-grained channel correlations. Specifically, we weightsum these four optimization objectives:

$$333 \quad \mathcal{L} = \text{RecLoss}^{\text{time}} + \lambda_1 \cdot \text{RecLoss}^{\text{freq}} + \lambda_2 \cdot \text{ClusteringLoss} + \lambda_3 \cdot \text{RegularLoss}, \quad (16)$$

335 where λ_1 , λ_2 , and λ_3 are empirical coefficients. We then
336 utilize a bi-level optimization
337 Algorithm 1 to iteratively update the *Mask Generator* and
338 other model parameters. Intuitively, the process optimizes
339 model parameters for current
340 channel correlations and then
341 discovers better channel correlations
342 for the optimized model
343 parameters, which facilitates the
344 refinement of channel correlations
345 in a continuous way.

348 3.5 ANOMALY SCORING
349

350 When calculating the anomaly score, the convention is to obey the point-to-point manner by as-
351 signing an anomaly score for each timestamp, thus mainly reflecting the point anomalies in the
352 time domain. To better quantify subsequence anomalies, existing methods often consider coarse-
353 grained window-granularity scoring, which adds a frequency anomaly score to each point in the
354 whole input window (Ren et al., 2019; Park et al., 2021; Zhang et al., 2022). However, they fail
355 to know the actual boundaries of subsequence anomalies, thus causing misjudgment or omission.
356 During scoring, we perform the patching operation in the input window with the stride length
357 equal to 1. In Figure 3, the shadow in the Time Series indicates a series of subsequence anomalies.
358 Take the calculation of the anomaly score for the red time point in the Time Series as
359 an example, we first calculate the time domain reconstruction error (RecLoss^{time}) between its
360 reconstructed value in the time domain and the true value using Equation 14, and denote the
361 result as the time domain anomaly score (time-score). At the same time, we collect all patches
362 containing the red time point, transform these patches into the frequency domain, and compute the
363 frequency reconstruction error (RecLoss^{freq}) between the reconstructed value and the true frequency-domain
364 value using Equation 15. The average frequency reconstruction error of all patches is then taken as the
365 frequency domain anomaly score (freq-score) for this red time point, as the average performs better than the
366 minimum or maximum value (Schmidl et al., 2022). Finally, we weightsum the time-score and freq-score point-to-point to
367 obtain the final anomaly score for the Time Series.

$$373 \quad \text{AnomalyScore} = \text{time-score} + \lambda_{\text{score}} \cdot \text{freq-score} \quad (17)$$

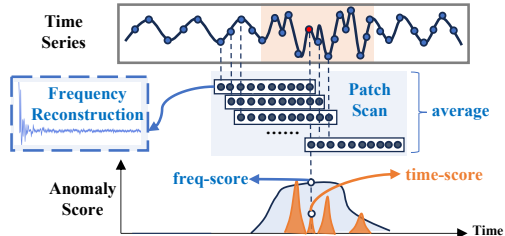
374 For ease of understanding, we provide an efficient implementation version of the calculation of freq-
375 score in Appendix A.5. Obviously, our method can reflect the real surroundings of each point by con-
376 sidering all possible subsequence anomalies around this point, thus achieving the point-granularity
377 alignment and showing strong sensitivity (Nam et al., 2024).

Algorithm 1 Bi-level Gradient Descent Optimization

```

1: Input: Model parameters  $\theta_{\text{model}}$ ,  $\theta_{\text{mask}}$ , learning rate  $\eta_{\text{model}}$ ,  $\eta_{\text{mask}}$ , number of iterations
    $\mathcal{N}_O$ ,  $\mathcal{N}_I$ , loss function  $\mathcal{L} = \text{RecLoss}^{\text{time}} + \lambda_1 \cdot \text{RecLoss}^{\text{freq}} + \lambda_2 \cdot \text{ClusteringLoss}$ 
   +  $\lambda_3 \cdot \text{RegularLoss}$ 
2: Initialize:  $\theta_{\text{model}} \leftarrow$  initial value,  $\theta_{\text{mask}} \leftarrow$  initial value
3: For  $i = 1$  to  $\mathcal{N}_O$ 
4:   Outer Loop: Update the mask generator parameters
5:      $\theta_{\text{mask}} \leftarrow \theta_{\text{mask}} - \eta_{\text{mask}} \cdot \nabla_{\theta_{\text{mask}}} \mathcal{L}(\theta_{\text{model}}, \theta_{\text{mask}})$   $\triangleright$  Update the Mask Generator
6:     For  $j = 1$  to  $\mathcal{N}_I$ 
7:       Inner Loop: Update the model parameters
8:          $\theta_{\text{model}} \leftarrow \theta_{\text{model}} - \eta_{\text{model}} \cdot \nabla_{\theta_{\text{model}}} \mathcal{L}(\theta_{\text{model}}, \theta_{\text{mask}})$   $\triangleright$  Update the model
9:       EndFor
10:    EndFor
11:   Output: Optimized parameters  $\theta_{\text{model}}, \theta_{\text{mask}}$ 

```



378 Figure 3: Proposed Anomaly Scoring.

378 **4 EXPERIMENTS**
 379

380 **Datasets** We conduct experiments using 9 real-world datasets and 12 synthetic datasets (TODS
 381 datasets) to assess the performance of CATCH, more details of the benchmark datasets are included
 382 in Appendix A.1. The synthetic datasets are generated using the method reported in (Lai et al.,
 383 2021). Please refer to Appendix A.6 for specific implementation. We report the results on 9 real-
 384 world MTSAD datasets, including MSL, PSM, SMD, CICIDS, CallIt2, NYC, Creditcard, GECCO
 385 and Genesis in the main text. We also report the mean results of the 6 types of synthetic anomalies.
 386 The complete results can be found in the Appendix C.

387 **Baselines** We comprehensively compare our model against 14 baselines, including the latest state-
 388 of-the-art (SOTA) models. These baselines feature the 2024 SOTA iTransformer (iTrans) (Liu et al.,
 389 2024), ModernTCN (Modern) (Luo & Wang, 2024), and DualTF (Nam et al., 2024), along with the
 390 2023 SOTA Anomaly Transformer (ATrans) (Xu et al., 2021), DCdetector (DC) (Yang et al., 2023b),
 391 TimesNet (TsNet) (Wu et al., 2022), PatchTST (Patch) (Nie et al., 2023), DLinear (DLin) (Zeng
 392 et al., 2023), NLinear (NLin) (Zeng et al., 2023), and AutoEncoder (AE) (Sakurada & Yairi, 2014).
 393 Additionally, we include non-learning methods such as One-Class SVM (OCSVM)(Schölkopf et al.,
 394 1999), Isolation Forest (IF)(Liu et al., 2008), Principal Component Analysis (PCA) (Shyu et al.,
 395 2003), and HBOS (Goldstein & Dengel, 2012).

396 **Setup** To keep consistent with previous works, we adopt Label-based metric: Affiliated-F1-
 397 score (*Aff-F*) (Huet et al., 2022) and Score-based metric: Area under the Receiver Operating
 398 Characteristics Curve (*ROC*) (Fawcett, 2006) as evaluation metrics. We report the algorithm per-
 399 formance under a total of 16 evaluation metrics in the Appendix C, and the details of the 16 metrics
 400 can be found in Appendix A.2. More implementation details are presented in the Appendix A.3.

401 **4.1 MAIN RESULTS**
 402

403 We first evaluate CATCH with 14 competitive baselines on 9 real-world multivariate and 6 types
 404 of synthetic multivariate datasets generated by the methods reported in TODS (Lai et al., 2021)
 405 as shown in Table 2. It can be seen that our proposed CATCH achieves SOTA results under the
 406 widely used Affiliated-F1-score metric in all benchmark datasets. Besides, CATCH has the highest
 407 AUC-ROC values on all datasets. It means that our model performs well in the false-positive and
 408 true-positive rates under various pre-selected thresholds, which is important for real-world appli-
 409 cations. CATCH effectively handles both point (Contextual, Global) and subsequence (Seasonal,
 410 Shapelet, Trend, Mixture) anomalies while showing greater improvement in detecting the sub-
 411 sequence anomalies. In addition, as shown in Table 3, CATCH’s performance on other metrics mostly
 412 remains at the forefront, further validating the robustness of our algorithm.

413 **4.2 MODEL ANALYSIS**
 414

415 **Ablation study**
 416

417 To ascertain the impact of different modules within CATCH, we per-
 418 form ablation studies focusing on the
 419 following components: (1) Substitute
 420 the channel correlation discover-
 421 ing mechanism with fixed Chan-
 422 nel Strategies. (2) Delete one of
 423 the four optimization objectives sep-
 424 arately. (3) Remove the patching op-
 425 eration during training process. (4)
 426 Replace the Scoring technique with
 427 others. (5) Replace the bi-level op-
 428 timization process with a normal pro-
 429 cess to optimize the *Mask Generator*
 430 and model simultaneously. Table 4 illus-
 431 trates the unique impact of each module. We have the follow-
 432 ing observations: 1) Compared to the Channel-Independent (CI) Strategy, considering the rela-
 433 tionships between variables using Channel Dependent (CD) Strategy or random masking yields better

Table 4: Ablation studies for CATCH in terms of the highest AUC-ROC highlighted in bold.

Variations		CICIDS	CallIt2	GECCO	MSL	SMD	Avg
Channel Correlation	CI	0.649	0.806	0.912	0.625	0.782	0.755
	CD	0.735	0.818	0.955	0.657	0.787	0.790
	Random	0.742	0.807	0.945	0.631	0.784	0.782
Optimization Objectives	w/o RecLoss ^{time}	0.784	0.827	0.953	0.652	0.766	0.796
	w/o RecLoss ^{freq}	0.663	0.825	0.96	0.608	0.745	0.760
	w/o ClusteringLoss	0.775	0.822	0.958	0.644	0.791	0.798
	w/o RegularLoss	0.788	0.830	0.966	0.657	0.802	0.809
Training w/o Patching		0.747	0.802	0.947	0.632	0.777	0.781
Scoring Technique	point + window score	0.751	0.743	0.952	0.653	0.794	0.775
	w/o point score	0.688	0.808	0.960	0.622	0.781	0.770
	w/o patch score	0.763	0.780	0.956	0.648	0.785	0.787
w/o bi-level optimization		0.791	0.833	0.965	0.658	0.809	0.811
CATCH (ours)		0.795	0.838	0.970	0.664	0.811	0.816

432
 433 Table 2: Average A-R (AUC-ROC) and Aff-F (Affiliated-F1) accuracy measures for 9 real-world
 434 datasets and 6 synthetic datasets of different types of anomalies. The best results are highlighted in
 435 bold, and the second-best results are underlined.
 436

Dataset	Metric	CATCH	Modern	<i>i</i> Trans	DualTF	ATrans	DC	TsNet	Patch	DLin	NLin	AE	Ocsvm	IF	PCA	Hbos
CICIDS	Aff-F	0.787	0.654	<u>0.708</u>	0.692	0.560	0.664	0.657	0.660	0.669	0.243	0.693	0.604	0.619	0.542	
	A-R	0.795	0.697	0.692	0.603	0.528	0.638	0.732	0.716	0.751	0.691	0.629	0.537	<u>0.787</u>	0.601	0.760
Callt2	Aff-F	0.835	0.780	<u>0.812</u>	0.751	0.729	0.697	0.794	0.793	0.793	0.757	0.587	0.783	0.402	0.768	0.756
	A-R	0.838	0.676	0.791	0.574	0.533	0.527	0.771	<u>0.808</u>	0.752	0.695	0.767	0.804	0.775	0.790	0.798
Credit	Aff-F	0.750	0.744	0.713	0.663	0.650	0.632	0.744	<u>0.746</u>	0.738	0.742	0.561	0.714	0.634	0.710	0.695
	A-R	0.958	0.957	0.934	0.703	0.552	0.504	<u>0.957</u>	0.957	0.954	0.948	0.909	0.953	0.860	0.871	0.951
GECCO	Aff-F	0.908	0.893	0.839	0.701	0.782	0.687	0.894	<u>0.906</u>	0.893	0.882	0.823	0.666	0.424	0.785	0.708
	A-R	0.970	0.952	0.795	0.714	0.516	0.555	<u>0.954</u>	0.949	0.947	0.936	0.769	0.804	0.619	0.711	0.557
Genesis	Aff-F	0.896	0.833	<u>0.891</u>	0.810	0.856	0.776	0.864	0.856	0.856	0.829	0.854	0.677	0.788	0.814	0.721
	A-R	0.974	0.676	0.690	0.937	<u>0.947</u>	0.659	0.913	0.685	0.696	0.755	0.931	0.733	0.549	0.815	0.897
MSL	Aff-F	0.740	0.726	0.710	0.588	0.692	0.694	<u>0.734</u>	0.724	0.725	0.723	0.625	0.641	0.584	0.678	0.680
	A-R	0.664	0.633	0.611	0.576	0.508	0.507	0.613	<u>0.637</u>	0.624	0.592	0.562	0.524	0.552	0.574	
NYC	Aff-F	0.994	0.769	0.684	0.708	0.853	<u>0.862</u>	0.794	<u>0.776</u>	0.828	0.819	0.689	0.667	0.648	0.680	0.675
	A-R	0.816	0.466	0.640	0.633	0.671	0.549	<u>0.791</u>	0.709	0.768	0.671	0.504	0.456	0.475	0.666	0.446
PSM	Aff-F	0.859	0.825	<u>0.854</u>	0.725	0.710	0.682	0.842	0.831	0.831	0.843	0.707	0.531	0.620	0.702	0.658
	A-R	0.652	0.593	0.592	0.600	0.514	0.501	0.592	0.586	0.580	0.585	<u>0.650</u>	0.619	0.542	0.648	0.620
SMD	Aff-F	0.847	0.840	0.827	0.679	0.724	0.675	0.831	<u>0.845</u>	0.841	0.844	0.439	0.742	0.626	0.738	0.629
	A-R	0.811	0.722	0.745	0.631	0.508	0.502	0.727	<u>0.736</u>	0.728	0.738	<u>0.774</u>	0.602	0.664	0.679	0.626
Contextual	Aff-F	0.823	0.619	<u>0.802</u>	0.635	0.601	0.597	0.666	0.766	0.780	0.700	0.755	0.696	0.679	0.475	0.481
	A-R	0.910	0.562	0.905	0.598	0.546	0.525	<u>0.908</u>	0.854	0.700	0.530	0.896	0.711	0.821	0.538	0.464
Global	Aff-F	0.949	0.748	0.922	0.649	0.656	0.567	0.910	<u>0.940</u>	0.928	0.808	0.919	0.849	0.912	0.704	0.528
	A-R	0.997	0.873	0.976	0.595	0.564	0.514	0.989	0.992	0.979	0.675	0.996	<u>0.996</u>	0.938	0.758	0.608
Seasonal	Aff-F	0.997	0.681	0.992	0.776	0.788	0.859	0.992	0.989	<u>0.993</u>	0.951	0.927	0.805	0.938	0.637	0.673
	A-R	0.998	0.512	0.946	0.701	0.584	0.644	0.958	0.922	0.823	0.623	0.949	0.829	0.918	0.437	0.516
Shapelet	Aff-F	0.985	0.675	0.961	0.692	0.699	0.737	0.941	0.933	<u>0.961</u>	0.759	0.871	0.771	0.887	0.683	0.640
	A-R	0.970	0.522	0.864	0.573	0.519	0.597	<u>0.877</u>	0.818	0.684	0.563	0.865	0.655	0.748	0.517	0.337
Trend	Aff-F	0.916	0.734	0.901	0.677	0.584	0.765	0.897	0.888	0.721	0.830	0.699	0.691	<u>0.914</u>	0.693	0.669
	A-R	0.892	0.612	0.847	0.524	0.500	0.569	0.858	0.835	0.671	0.642	0.482	0.471	<u>0.878</u>	0.484	0.468
Mixture	Aff-F	0.892	0.856	0.862	0.652	0.641	0.709	0.863	0.879	0.727	0.839	0.673	0.676	<u>0.881</u>	0.676	0.667
	A-R	0.931	0.763	0.854	0.570	0.522	0.516	0.861	0.863	0.767	0.749	0.493	0.475	<u>0.911</u>	0.517	0.531

434
 435 Table 3: Multi-metrics results on three real-world multivariate datasets. The best ones are in Bold.
 436

Dataset	Method	Acc	P	R	F1	R-P	R-R	R-F	Aff-P	Aff-R	Aff-F	A-R	A-P	R-A-R	R-A-P	V-ROC	V-PR
GECCO	TimesNet	0.984	0.379	0.804	0.516	0.053	0.782	0.099	0.810	0.997	0.894	0.954	0.410	0.977	0.428	0.974	0.429
	ModernTCN	0.984	0.373	0.779	0.504	0.086	0.644	0.152	0.808	0.998	0.893	0.952	0.447	0.978	0.459	0.975	0.461
	CATCH (ours)	0.984	0.380	0.818	0.518	0.065	0.795	0.119	0.832	0.998	0.908	0.970	0.418	0.990	0.473	0.987	0.465
MSL	TimesNet	0.855	0.166	0.093	0.119	0.130	0.224	0.164	0.589	0.973	0.734	0.613	0.146	0.701	0.231	0.692	0.227
	ModernTCN	0.857	0.166	0.090	0.117	0.129	0.194	0.155	0.578	0.975	0.726	0.633	0.146	0.708	0.224	0.701	0.220
	CATCH (ours)	0.853	0.185	0.117	0.143	0.150	0.241	0.185	0.599	0.966	0.740	0.664	0.167	0.747	0.260	0.735	0.256
SMD	TimesNet	0.931	0.176	0.181	0.178	0.110	0.385	0.171	0.745	0.938	0.831	0.727	0.141	0.747	0.140	0.746	0.140
	ModernTCN	0.931	0.151	0.145	0.148	0.092	0.378	0.148	0.755	0.948	0.840	0.722	0.130	0.743	0.130	0.742	0.130
	CATCH (ours)	0.918	0.194	0.305	0.237	0.095	0.478	0.158	0.773	0.938	0.847	0.811	0.172	0.800	0.159	0.797	0.159

437 results, with the random masking performing worse than the CD method. Ours outperforms the CD
 438 method, further demonstrating the effectiveness of the channel correlation discovering mechanism.
 439 2) Removing any of the four optimization objectives leads to a decline in model performance, with
 440 the most significant drop occurring when the frequency loss is removed. This fully demonstrates
 441 the rationality and effectiveness of the four optimization objectives. 3) When the patching operation
 442 is removed during training and replaced with a window-based approach to model the relationships
 443 between variables, the model performance significantly decreases. This indicates that the patching
 444 operation captures fine-grained frequency information, which is more conducive to anomaly
 445 detection. 4) When replacing the combination of point-granularity temporal anomaly scores and
 446 patch-wise point-aligned frequency anomaly scores with the combination of point-granularity tem-
 447 poral anomaly scores and window-granularity frequency anomaly scores, or when using only one
 448 of them, the model performance decreases in both cases. This indicates our Scoring technique
 449 shows stronger sensitivity in detecting anomalies. 5) When using a normal optimization process, the
 450 model performance also decreases consistently, which provides empirical evidence for the bi-level
 451 optimization.

452

453 **Parameter Sensitivity** We also study the parameter sensitivity of the CATCH. Figure 4a shows
 454 the performance under different input window sizes. As discussed, a single point can not be taken
 455 as an instance in time series. Window segmentation is widely used in the analysis, and window
 456 size is a significant parameter. For our primary evaluation, the window size is usually set as 96
 457 or 192. Besides, we adopt the score weight in section 3.5 to trade off the temporal score and the
 458 frequency score—see Figure 4b. We find that score weight is mostly stable and easy to tune in the
 459 range of 0.01 to 0.1. Figure 4c and Figure 4d present that our model is stable to the Training patch size
 460 and Testing patch size respectively over extensive datasets. Note that a small patch size indicates
 461 a larger memory cost and a larger patch number. Especially, only considering the performance,
 462

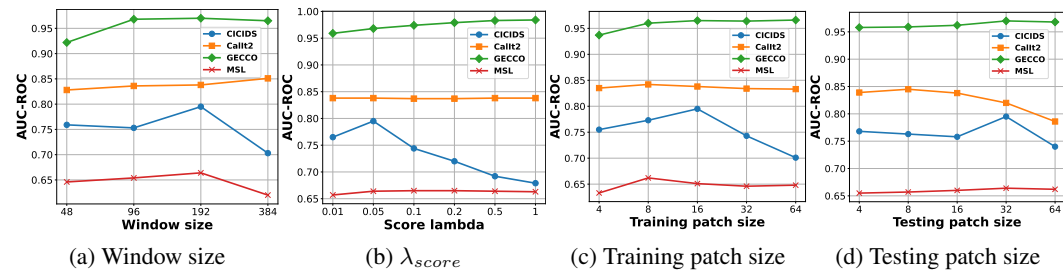


Figure 4: Parameter sensitivity studies of main hyper-parameters in CATCH.

its relationship to the patch size can be determined by the data pattern. For example, our model performs better when the traing patch size is 8 for the MSL dataset, the testing patch size is 32 for the CICIDS dataset.

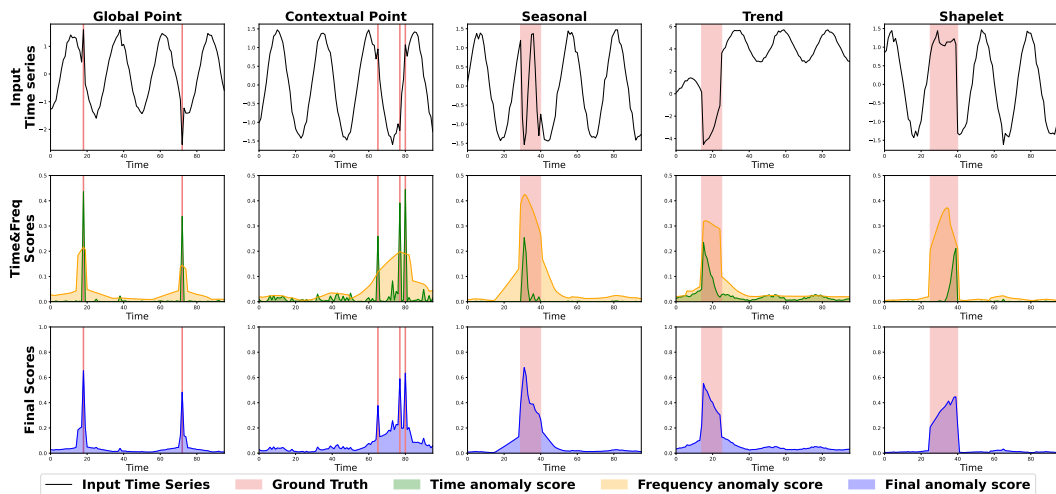


Figure 5: Visualization of dual-domain anomaly scores from CATCH for different categories of point and subsequence anomalies using the TODS dataset.

Anomaly criterion visualization We show how CATCH works by visualizing different anomalies in Figure 5. This figure showcases CATCH’s performance across five anomaly categories (Lai et al., 2021) on the TODS dataset, with temporal and frequency scores displayed in the second row, and the final anomaly scores in the third row. For point anomalies (first and second columns), the temporal scores exhibit sharp increases at the true anomaly locations, dominating the total scores. In contrast, for subsequence anomalies (third, fourth, and fifth columns), frequency scores remain elevated across the entire anomaly interval, show strong sensitivity to the actual boundaries of subsequence anomalies and compensate for the insensitivity of the temporal scores. Consequently, each domain contributes uniquely, allowing the final anomaly scores to accurately capture both point and subsequence anomalies.

5 CONCLUSION

In this paper, we propose a novel framework, CATCH, capable of simultaneously detecting both point and subsequence anomalies. To sum up, it patchifys the frequency domain for fine-grained insights into frequency bands, flexibly perceives and discovers appropriate channel correlations, optimizes the attention mechanism for both robustness and capacity with a bi-level optimization algorithm. These innovative mechanisms collectively empower CATCH to precisely detect both point and subsequence anomalies. Comprehensive experiments on real-world and synthetic datasets demonstrate that CATCH achieves state-of-the-art performance.

540 **6 REPRODUCIBILITY**
 541

542 The study meets reproducibility requirements. Specifically, the datasets are available
 543 for download in a standardized format from here, and the code can be browsed at
 544 <https://anonymous.4open.science/r/CATCH-E535>. It may take some time to download the datasets,
 545 please wait patiently.
 546

547 **REFERENCES**
 548

- 549 Markus M Breunig, Hans-Peter Kriegel, Raymond T Ng, and Jörg Sander. Lof: identifying density-
 550 based local outliers. In *Proceedings of the 2000 ACM SIGMOD international conference on*
 551 *Management of data*, pp. 93–104, 2000.
- 552 E Oran Brigham and RE Morrow. The fast fourier transform. *IEEE spectrum*, 4(12):63–70, 1967.
- 554 Tri Dao and Albert Gu. Transformers are ssms: Generalized models and efficient algorithms through
 555 structured state space duality. *arXiv preprint arXiv:2405.21060*, 2024.
- 557 Jesse Davis and Mark Goadrich. The relationship between precision-recall and roc curves. In
 558 *Proceedings of the international conference on machine learning*, pp. 233–240, 2006.
- 559 Ailin Deng and Bryan Hooi. Graph neural network-based anomaly detection in multivariate time
 560 series. In *Proceedings of the AAAI conference on artificial intelligence*, volume 35, pp. 4027–
 561 4035, 2021.
- 563 Tom Fawcett. An introduction to roc analysis. *Pattern recognition letters*, 27(8):861–874, 2006.
- 564 Markus Goldstein and Andreas Dengel. Histogram-based outlier score (hbos): A fast unsupervised
 565 anomaly detection algorithm. *KI 2012 - German Conference on Artificial Intelligence: poster and*
 566 *demo track*, 1:59–63, 2012.
- 568 Albert Gu and Tri Dao. Mamba: Linear-time sequence modeling with selective state spaces. *arXiv*
 569 *preprint arXiv:2312.00752*, 2023.
- 571 Xiaojun Guo, Yifei Wang, Tianqi Du, and Yisen Wang. Contranorm: A contrastive learning per-
 572 spective on oversmoothing and beyond. In *The Eleventh International Conference on Learning*
 573 *Representations*, 2023.
- 574 Lu Han, Han-Jia Ye, and De-Chuan Zhan. The capacity and robustness trade-off: Revisiting the
 575 channel independent strategy for multivariate time series forecasting. *IEEE Transactions on*
 576 *Knowledge and Data Engineering*, 2024.
- 578 Kaiming He, Haoqi Fan, Yuxin Wu, Saining Xie, and Ross Girshick. Momentum contrast for
 579 unsupervised visual representation learning. In *Proceedings of the IEEE/CVF conference on*
 580 *computer vision and pattern recognition*, pp. 9729–9738, 2020.
- 581 Alexis Huet, Jose Manuel Navarro, and Dario Rossi. Local evaluation of time series anomaly de-
 582 tection algorithms. In *Proceedings of the ACM SIGKDD international conference on knowledge*
 583 *discovery & data mining*, pp. 635–645, 2022.
- 585 Eric Jang, Shixiang Gu, and Ben Poole. Categorical reparametrization with gumble-softmax. In
 586 *International Conference on Learning Representations (ICLR 2017)*. OpenReview.net, 2017.
- 587 Tung Kieu, Bin Yang, and Christian S Jensen. Outlier detection for multidimensional time series
 588 using deep neural networks. In *2018 19th IEEE International Conference on Mobile Data Man-*
 589 *agement (MDM)*. IEEE, 2018.
- 591 Tung Kieu, Bin Yang, Chenjuan Guo, and Christian S Jensen. Outlier detection for time series
 592 with recurrent autoencoder ensembles. In *Proceedings of the Twenty-Eighth International Joint*
 593 *Conference on Artificial Intelligence*. International Joint Conferences on Artificial Intelligence
 Organization, 2019.

- 594 Kwei-Herng Lai, Daochen Zha, Junjie Xu, Yue Zhao, Guanchu Wang, and Xia Hu. Revisiting time
 595 series outlier detection: Definitions and benchmarks. In *Proceedings of the conference on neural*
 596 *information processing systems datasets and benchmarks track (round 1)*, 2021.
- 597
- 598 Xing Li, Qiquan Shi, Gang Hu, Lei Chen, Hui Mao, Yiyuan Yang, Mingxuan Yuan, Jia Zeng,
 599 and Zhuo Cheng. Block access pattern discovery via compressed full tensor transforme-
 600 iclr2025conferencer. In *Proceedings of the 30th ACM International Conference on Information*
 601 *& Knowledge Management*, pp. 957–966, 2021.
- 602 Fei Tony Liu, Kai Ming Ting, and Zhi-Hua Zhou. Isolation forest. In *Proceedings of the 2008 IEEE*
 603 *international conference on data mining*, pp. 413–422, 2008.
- 604
- 605 Yong Liu, Tengge Hu, Haoran Zhang, Haixu Wu, Shiyu Wang, Lintao Ma, and Mingsheng Long.
 606 itransformer: Inverted transformers are effective for time series forecasting. In *The Twelfth Inter-*
 607 *national Conference on Learning Representations*, 2024.
- 608 Donghao Luo and Xue Wang. Moderntcn: A modern pure convolution structure for general time
 609 series analysis. In *The Twelfth International Conference on Learning Representations*, 2024.
- 610
- 611 Youngeun Nam, Susik Yoon, Yooju Shin, Minyoung Bae, Hwanjun Song, Jae-Gil Lee, and
 612 Byung Suk Lee. Breaking the time-frequency granularity discrepancy in time-series anomaly
 613 detection. In *Proceedings of the ACM on Web Conference 2024*, pp. 4204–4215, 2024.
- 614 Yuqi Nie, Nam H Nguyen, Phanwadee Sinthong, and Jayant Kalagnanam. A time series is worth 64
 615 words: Long-term forecasting with transformers. In *The Eleventh International Conference on*
 616 *Learning Representations*, 2023.
- 617 John Paparrizos, Paul Boniol, Themis Palpanas, Ruey S Tsay, Aaron Elmore, and Michael J
 618 Franklin. Volume Under the Surface: A New Accuracy Evaluation Measure for Time-Series
 619 Anomaly Detection. *Proceedings of the VLDB Endowment*, 15(11):2774–2787, 2022a.
- 620
- 621 John Paparrizos, Yuhao Kang, Paul Boniol, Ruey S Tsay, Themis Palpanas, and Michael J Franklin.
 622 Tsb-uad: an end-to-end benchmark suite for univariate time-series anomaly detection. *Proce-*
 623 *dings of the VLDB Endowment*, 15(8):1697–1711, 2022b.
- 624 Namuk Park and Songkuk Kim. How do vision transformers work? In *10th International Confer-*
 625 *ence on Learning Representations, ICLR 2022*, 2022.
- 626
- 627 Yong-chan Park, Jun-Gi Jang, and U Kang. Fast and accurate partial fourier transform for time
 628 series data. In *Proceedings of the 27th ACM SIGKDD Conference on Knowledge Discovery &*
 629 *Data Mining*, pp. 1309–1318, 2021.
- 630 Adam Paszke, Sam Gross, Francisco Massa, Adam Lerer, James Bradbury, Gregory Chanan, Trevor
 631 Killeen, Zeming Lin, Natalia Gimelshein, Luca Antiga, et al. Pytorch: An imperative style,
 632 high-performance deep learning library. *Advances in Neural Information Processing Systems*, 32,
 633 2019.
- 634
- 635 Xihao Piao, Zheng Chen, Taichi Murayama, Yasuko Matsubara, and Yasushi Sakurai. Fredformer:
 636 Frequency debiased transformer for time series forecasting. In *Proceedings of the 30th ACM*
 637 *SIGKDD Conference on Knowledge Discovery and Data Mining*, pp. 2400–2410, 2024.
- 638 Xiangfei Qiu, Jilin Hu, Lekui Zhou, Xingjian Wu, Junyang Du, Buang Zhang, Chenjuan Guo, Aoy-
 639 ing Zhou, Christian S. Jensen, Zhenli Sheng, and Bin Yang. Tfb: Towards comprehensive and fair
 640 benchmarking of time series forecasting methods. *Proc. VLDB Endow.*, 17(9):2363–2377, 2024.
- 641 Sridhar Ramaswamy, Rajeev Rastogi, and Kyuseok Shim. Efficient algorithms for mining outliers
 642 from large data sets. In *Proceedings of the 2000 ACM SIGMOD international conference on*
 643 *management of data*, pp. 427–438, 2000.
- 644
- 645 Hansheng Ren, Bixiong Xu, Yujing Wang, Chao Yi, Congrui Huang, Xiaoyu Kou, Tony Xing,
 646 Mao Yang, Jie Tong, and Qi Zhang. Time-series anomaly detection service at microsoft. In
 647 *Proceedings of the 25th ACM SIGKDD international conference on knowledge discovery & data*
 648 *mining*, pp. 3009–3017, 2019.

- 648 Mayu Sakurada and Takehisa Yairi. Anomaly detection using autoencoders with nonlinear dimen-
 649 sionality reduction. In *Proceedings of the MLSDA 2014 2nd workshop on machine learning for*
 650 *sensory data analysis*, pp. 4–11, 2014.
- 651 Sebastian Schmidl, Phillip Wenig, and Thorsten Papenbrock. Anomaly detection in time series: a
 652 comprehensive evaluation. *Proceedings of the VLDB Endowment*, 15(9):1779–1797, 2022.
- 653 Bernhard Schölkopf, Robert C Williamson, Alex Smola, John Shawe-Taylor, and John Platt. Support
 654 vector method for novelty detection. *Advances in neural information processing systems*, 12,
 655 1999.
- 656 Mei-Ling Shyu, Shu-Ching Chen, Kanoksri Sarinnapakorn, and LiWu Chang. A novel anomaly
 657 detection scheme based on principal component classifier. In *Proceedings of the IEEE foundations*
 658 *and new directions of data mining workshop*, pp. 172–179, 2003.
- 659 Dongjin Song, Ning Xia, Wei Cheng, Haifeng Chen, and Dacheng Tao. Deep r-th root of rank
 660 supervised joint binary embedding for multivariate time series retrieval. In *Proceedings of the 24th*
 661 *ACM SIGKDD International Conference on Knowledge Discovery & Data Mining*, pp. 2229–
 662 2238, 2018.
- 663 Nesime Tatbul, Tae Jun Lee, Stan Zdonik, Mejbah Alam, and Justin Gottschlich. Precision and
 664 recall for time series. *Advances in neural information processing systems*, 31, 2018.
- 665 A Vaswani. Attention is all you need. *Advances in Neural Information Processing Systems*, 2017.
- 666 Hao Wang, Licheng Pan, Zhichao Chen, Degui Yang, Sen Zhang, Yifei Yang, Xinggao Liu, Haox-
 667 uan Li, and Dacheng Tao. Fredf: Learning to forecast in frequency domain. *arXiv preprint*
 668 *arXiv:2402.02399*, 2024.
- 669 Peihao Wang, Wenqing Zheng, Tianlong Chen, and Zhangyang Wang. Anti-oversmoothing in deep
 670 vision transformers via the fourier domain analysis: From theory to practice. In *International*
 671 *Conference on Learning Representations*, 2022.
- 672 Qingsong Wen, Linxiao Yang, Tian Zhou, and Liang Sun. Robust time series analysis and appli-
 673 cations: An industrial perspective. In *Proceedings of the 28th ACM SIGKDD Conference on*
 674 *Knowledge Discovery and Data Mining*, pp. 4836–4837, 2022.
- 675 Haixu Wu, Tengge Hu, Yong Liu, Hang Zhou, Jianmin Wang, and Mingsheng Long. Timesnet:
 676 Temporal 2d-variation modeling for general time series analysis. In *The Eleventh International*
 677 *Conference on Learning Representations*, 2022.
- 678 Jiehui Xu, Haixu Wu, Jianmin Wang, and Mingsheng Long. Anomaly transformer: Time series
 679 anomaly detection with association discrepancy. In *International Conference on Learning Repre-*
 680 *sentations*, 2021.
- 681 Zhijian Xu, Ailing Zeng, and Qiang Xu. Fits: Modeling time series with 10k parameters. In *The*
 682 *Twelfth International Conference on Learning Representations*.
- 683 Yiyuan Yang, Rongshang Li, Qiquan Shi, Xijun Li, Gang Hu, Xing Li, and Mingxuan Yuan. Sgdp:
 684 A stream-graph neural network based data prefetcher. In *2023 International Joint Conference on*
 685 *Neural Networks (IJCNN)*, pp. 1–8. IEEE, 2023a.
- 686 Yiyuan Yang, Chaoli Zhang, Tian Zhou, Qingsong Wen, and Liang Sun. Dcdetector: Dual attention
 687 contrastive representation learning for time series anomaly detection. In *Proceedings of the 29th*
 688 *ACM SIGKDD Conference on Knowledge Discovery and Data Mining*, pp. 3033–3045, 2023b.
- 689 Chin-Chia Michael Yeh, Yan Zhu, Liudmila Ulanova, Nurjahan Begum, Yifei Ding, Hoang Anh
 690 Dau, Diego Furtado Silva, Abdullah Mueen, and Eamonn Keogh. Matrix profile i: all pairs
 691 similarity joins for time series: a unifying view that includes motifs, discords and shapelets. In
 692 *Proceedings of the 2016 IEEE international conference on data mining*, pp. 1317–1322, 2016.
- 693 Ailing Zeng, Muxi Chen, Lei Zhang, and Qiang Xu. Are transformers effective for time series
 694 forecasting? In *Proceedings of the AAAI conference on artificial intelligence*, volume 37, pp.
 695 11121–11128, 2023.

702 Chaoli Zhang, Tian Zhou, Qingsong Wen, and Liang Sun. Tfad: A decomposition time series
703 anomaly detection architecture with time-frequency analysis. In *Proceedings of the 31st ACM*
704 *International Conference on Information & Knowledge Management*, pp. 2497–2507, 2022.

705 Chuxu Zhang, Dongjin Song, Yuncong Chen, Xinyang Feng, Cristian Lumezanu, Wei Cheng,
706 Jingchao Ni, Bo Zong, Haifeng Chen, and Nitesh V Chawla. A deep neural network for un-
707 supervised anomaly detection and diagnosis in multivariate time series data. In *Proceedings of*
708 *the AAAI conference on artificial intelligence*, volume 33, pp. 1409–1416, 2019.

710 Hang Zhao, Yujing Wang, Juanyong Duan, Congrui Huang, Defu Cao, Yunhai Tong, Bixiong Xu,
711 Jing Bai, Jie Tong, and Qi Zhang. Multivariate time-series anomaly detection via graph attention
712 network. In *2020 IEEE international conference on data mining (ICDM)*, pp. 841–850. IEEE,
713 2020.

714

715

716

717

718

719

720

721

722

723

724

725

726

727

728

729

730

731

732

733

734

735

736

737

738

739

740

741

742

743

744

745

746

747

748

749

750

751

752

753

754

755

756 **A EXPERIMENTAL DETAILS**

757

758 **A.1 DATASETS**

759

760 Table 5: Statistics of multivariate datasets (AR: anomaly ratio).

761

Dataset	Domain	Dim	AR (%)	Avg Total Length	Avg Test Length	Description
MSL	Spacecraft	55	5.88	132,046	73,729	Spacecraft incident and anomaly data from the MSL Curiosity rover
PSM	Server Machine	25	11.07	220,322	87,841	A dataset collected from multiple application server nodes at eBay
SMD	Server Machine	38	2.08	1,416,825	708,420	Telemetry dataset collected from 28 different server machines at a large Internet company
Creditcard	Finance	29	0.17	284,807	142,404	Credit card dataset includes a subset of online transactions that occurred over two days
GECCO	Water treatment	9	1.25	138,521	69,261	Water quality dataset published in the GECCO Industrial Challenge
CICIDS	Web	72	1.28	170,231	85,116	Network traffic data from CICFlowMeter with 80+ features and attack labels
CalIt2	Visitors flowrate	2	4.09	5,040	2,520	Person flow dataset records the movement of people in and out of a building over 15 days
Genesis	Machinery	18	0.31	16,220	12,616	A sensor and control signals dataset collected from cyber-physical production systems
NYC	Transport	3	0.57	17,520	4,416	Transportation dataset provides information on taxi and ride-hailing trips in New York
TODS	Synthetic	5	6.35	20,000	5,000	Including 6 anomaly types: global, contextual, shapelet, seasonal, trend, and mix anomalies

762
 763 In order to comprehensively evaluate the performance of CATCH, we evaluate 9 real-world datasets
 764 and 12 synthetic datasets which cover 8 domains. The anomaly ratio vary from 0.17% to 11.07%,
 765 the range of feature dimensions varies from 3 to 72, and the sequence length varies from 5,040
 766 to 1,416,825. This substantial diversity of the datasets enables comprehensive studies of MTSAD
 767 methods. Table 5 lists statistics of the 21 multivariate time series.

768 **A.2 METRICS**

769

770 The metrics we support can be divided into two categories: Score-based and Label-based.
 771 Label-based metrics includes Accuracy (Acc), Precision (P), Recall (R), F1-score ($F1$), Range-
 772 Precision ($R-P$), Range-Recall ($R-R$), Range-F1-score ($R-F$) (Tatbul et al., 2018), Precision@k,
 773 Affiliated-Precision ($Aff-P$), Affiliated-Recall ($Aff-R$), and Affiliated-F1-score ($Aff-F$) (Huet
 774 et al., 2022). Score-based metrics includes the Area Under the Precision-Recall Curve ($A-P$) (Davis
 775 & Goadrich, 2006), the Area under the Receiver Operating Characteristics Curve ($A-R$) (Fawcett,
 776 2006), the Range Area Under the Precision-Recall Curve ($R-A-P$), the Range Area under the Re-
 777 ceiver Operating Characteristics Curve ($R-A-R$) (Paparrizos et al., 2022a), the Volume Under the
 778 Surface of Precision-Recall ($V-PR$), and the Volume Under the Surface of Receiver Operating
 779 Characteristic ($V-ROC$) (Paparrizos et al., 2022a). As noted earlier, CATCH computes all metrics
 780 to provide a complete picture of each method. More implementation details are presented in the
 781 Appendix A.3.

782 **A.3 IMPLEMENTATION DETAILS**

783

784 The “*Drop Last*” issue is reported by several researchers (Qiu et al., 2024; Xu et al.). That is, in some
 785 previous works evaluating the model on test set with drop-last=True setting may cause additional
 786 errors related to test batch size. In our experiment, to ensure fair comparison in the future, we set
 787 the drop last to False for all baselines to avoid this issue.

788 All experiments are conducted using PyTorch (Paszke et al., 2019) in Python 3.8 and execute
 789 on an NVIDIA Tesla-A800 GPU. We employ the ADAM optimizer during training. Initially,
 790 the batch size is set to 32, with the option to reduce it by half (to a minimum of 8) in case
 791 of an Out-Of-Memory (OOM) situation. We do not use the “*Drop Last*” operation during test-
 792 ing. To ensure reproducibility and facilitate experimentation, datasets and code are available at:
 793 <https://anonymous.4open.science/r/CATCH-E535>.

801
 802
 803
 804
 805
 806
 807
 808
 809

810

811

812

A.4 MODEL HYPERPARAMETER SETTINGS

813

814 For each baseline method, we strictly follow the hyperparameter configurations recommended in
 815 their original papers. Additionally, we conduct hyperparameter searches on multiple sets and select
 816 the optimal configurations based on these evaluations to ensure a comprehensive and fair assessment
 817 of each method's performance.

818 The hyperparameters for the baseline methods are set as follows:

819

820

821

822

823

824

825

826

827

828

829

830

831

832

833

834

835

836

837

838

839

840

841

842

843

844

845

846

847

848

849

850

851

852

853

854

855

856

857

858

859

860

861

862

863

864 A.5 IMPLEMENTATION DETAILS OF SCORING
865

866 We provide an efficient implementation of Frequency-Enhanced Point-Granularity Scoring in Sec-
867 tion 3.5. We present the pseudo-code in Algorithm 2. Specifically, we adopt the scatter operation in
868 Pytorch to efficiently parallel the collection of patches to which each point belongs.
869

870

871 **Algorithm 2** Calculation of freq-score

```

872 from einops import rearrange
873 import torch
874
875 class frequency_criterion(torch.nn.Module):
876     def __init__(self, configs):
877         super(frequency_criterion, self).__init__()
878         # Define the frequency metric
879         self.metric = frequency_loss(configs, dim=1, keep_dim=True)
880         self.patch_size = configs.inference_patch_size
881         self.patch_stride = configs.inference_patch_stride
882         self.win_size = configs.seq_len
883         self.patch_num = int((self.win_size - self.patch_size) /
884                             self.patch_stride + 1)
885         self.padding_length = self.win_size - (self.patch_size
886                                             + (self.patch_num - 1) * self.patch_stride)
887
888     def forward(self, outputs, batch_y):
889
890         output_patch = outputs.unfold(dimension=1,
891                                     size=self.patch_size, step=self.patch_stride)
892
893         b, n, c, p = output_patch.shape
894         output_patch = rearrange(output_patch, 'b n c p -> (b n) p c')
895         y_patch = batch_y.unfold(dimension=1,
896                                 size=self.patch_size, step=self.patch_stride)
897         y_patch = rearrange(y_patch, 'b n c p -> (b n) p c')
898
899         main_part_loss = self.metric(output_patch, y_patch)
900
901         # Create the patches
902         main_part_loss = main_part_loss.repeat(1, self.patch_size, 1)
903         main_part_loss = rearrange(main_part_loss,
904                                     '(b n) p c -> b n p c', b=b)
905
906         # Calculate the overlapped indices
907         end_point = self.patch_size + (self.patch_num - 1) *
908                     self.patch_stride - 1
909         start_indices = np.array(range(0, end_point, self.patch_stride))
910         end_indices = start_indices + self.patch_size
911
912         indices = torch.tensor([range(start_indices[i], end_indices[i])
913                                for i in range(n)]).unsqueeze(0).unsqueeze(-1)
914         indices = indices.repeat(b, 1, 1, c).to(main_part_loss.device)
915
916         # Point-Granularity Alignment
917         main_loss = torch.zeros((b, n, self.win_size -
918                               self.padding_length, c)).to(main_part_loss.device)
919         main_loss.scatter_(dim=2, index=indices, src=main_part_loss)
920
921         non_zero_cnt = torch.count_nonzero(main_loss, dim=1)
922         main_loss = main_loss.sum(1) / non_zero_cnt
923
924         # Calculate the metric of the remained part
925         if self.padding_length > 0:
926             padding_loss = self.metric(outputs[:, -self.padding_length:, :],
927                                       batch_y[:, -self.padding_length:, :])
928             padding_loss = padding_loss.repeat(1, self.padding_length, 1)
929             total_loss = torch.concat([main_loss, padding_loss], dim=1)
930         else:
931             total_loss = main_loss
932
933         return total_loss

```

918 A.6 COMMAND USED FOR GENERATING THE SYNTHETIC DATASETS
919920 We use the provided source code (Lai et al., 2021) without alterations as demonstrated below, except
921 for adjusting the length parameter to generate a longer time series, to ensure a fair comparison.
922923 **Algorithm 3** TODS Synthesis

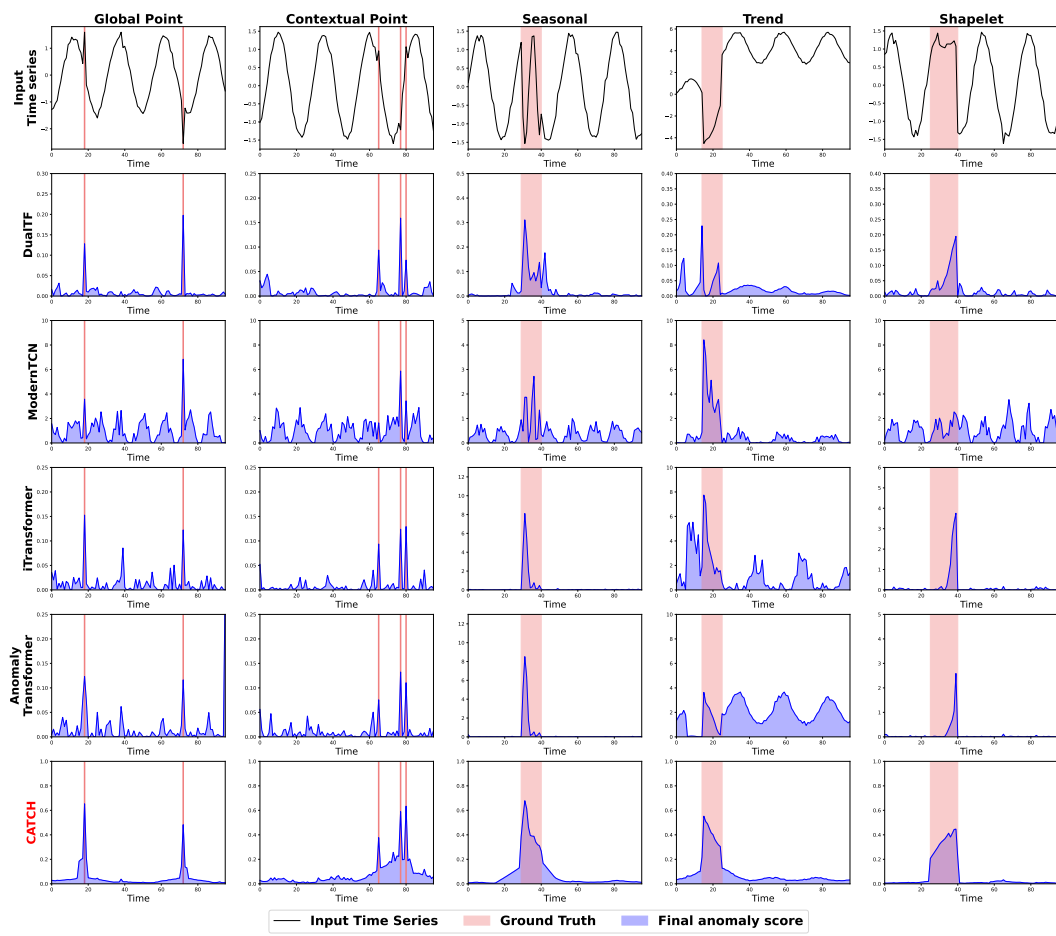
```

924 """
925 This code is based on the original implementation from the TODS project.
926 Original author: DATA Lab @ Rice University
927 Source URL: https://github.com/datamllab/tods
928 """
929 # Set base values and behavior types
930 DIM_NUM = 5
931 BEHAVIOR = [sine, cosine, sine, cosine, sine]
932 CONFIG = {"freq": 0.04, "coef": 1.5, "offset": 0.0, "noise_amp": 0.05}
933 VALUES = [0.145, 0.128, 0.094, 0.077, 0.111, 0.145, 0.179, 0.214, 0.214]
934
935 # Generate training data
936 train_data = MultivariateDataGenerator(dim=DIM_NUM, stream_length=20000,
937                                         behavior=BEHAVIOR, behavior_config=CONFIG)
938
939 # Generate test data
940 test_data = MultivariateDataGenerator(dim=DIM_NUM, stream_length=5000,
941                                         behavior=BEHAVIOR, behavior_config=CONFIG)
942
943 # Add anomalies based on the specified anomaly type
944 for i in range(DIM_NUM):
945     if anomaly_type == "global_anomaly":
946         test_data.point_global_outliers(dim_no=i, ratio=0.01, factor=3.5,
947                                         radius=5)
948     elif anomaly_type == "contextual_anomaly":
949         test_data.point_contextual_outliers(dim_no=i, ratio=0.01, factor=2.5,
950                                         radius=5)
951     elif anomaly_type == "shapelet_anomaly":
952         test_data.collective_global_outliers(dim_no=i, ratio=0.01, radius=5,
953                                             option='square', coef=1.5, noise_amp=0.03, level=20, freq=0.04,
954                                             base=VALUES, offset=0.0)
955     elif anomaly_type == "seasonal_anomaly":
956         test_data.collective_seasonal_outliers(dim_no=i, ratio=0.01, factor=3,
957                                         radius=5)
958     elif anomaly_type == "trend_anomaly":
959         test_data.collective_trend_outliers(dim_no=i, ratio=0.01, factor=0.5,
960                                         radius=5)
961     elif anomaly_type == "mixed_subsequence_anomaly":
962         test_data.collective_global_outliers(dim_no=i, ratio=0.006, radius=5,
963                                             option="square", coef=1.5, noise_amp=0.03, level=20, freq=0.04,
964                                             base=VALUES, offset=0.0)
965         test_data.collective_seasonal_outliers(dim_no=i, ratio=0.006, factor=3,
966                                         radius=5)
967         test_data.collective_trend_outliers(dim_no=i, ratio=0.006, factor=0.5,
968                                         radius=5)
969
970
971

```

972 B ADDITIONAL CASE STUDIES 973

974 As shown in Figure 6, we visualize the anomaly scores of various recent SOTAs to obtain an intu-
975 itive comparison of detecting accuracy. Our proposed CATCH shows most distinguishable anomaly
976 scores in detecting both point and subsequence anomalies.
977



1008 Figure 6: Visualization of anomaly scores from recent SOTAs for the TODS datasets.
1009
1010
1011
1012
1013
1014
1015
1016
1017
1018
1019
1020
1021
1022
1023
1024
1025

1026 C FULL EXPERIMENTAL RESULTS

1028 The full MTSAD results are provided in the following section due to the space limitation of the
 1029 main text. Tables 6, 7, 8, 9, and 10, show the (AUC-ROC, R-AUC-ROC, VUS-ROC), (AUC-PR,
 1030 R-AUC-PR, VUS-PR), (Accuracy, Precision, Recall, F1-score), (Range-Recall, Range-Precision,
 1031 Range-F1-score), (Affiliated-Precision, Affiliated-Recall, Affiliated-F1-score) results, respectively.

1032
 1033 Table 6: Average A-R (AUC-ROC), R-A-R (R-AUC-ROC) and V-ROC (VUS-ROC) accuracy mea-
 1034 sures for all datasets. The best results are highlighted in bold, and the second-best results are under-
 1035 lined.

Dataset	Metric	CATCH	Modern	iTrans	DualTF	ATrans	DC	TsNet	Patch	DLin	NLin	AE	Ocsvm	IF	PCA	HBOS
CICIDS	A-R	0.795	0.697	0.692	0.603	0.528	0.638	0.732	0.716	0.751	0.691	0.629	0.537	0.787	0.601	0.760
	R-A-R	<u>0.737</u>	0.637	0.584	0.434	0.392	0.492	0.684	0.650	0.692	0.609	0.574	0.481	0.739	0.478	0.720
	V-ROC	<u>0.743</u>	0.649	0.626	0.485	0.408	0.528	0.693	0.662	0.703	0.631	0.586	0.505	0.750	0.496	0.735
CallIt2	A-R	0.838	0.676	0.791	0.574	0.533	0.527	0.771	0.808	0.752	0.695	0.767	0.804	0.775	0.790	0.798
	R-A-R	0.854	0.726	0.817	0.666	0.523	0.505	0.807	0.830	0.794	0.743	0.798	0.840	0.818	0.796	0.847
	V-ROC	<u>0.848</u>	0.716	0.809	0.630	0.517	0.503	0.796	0.824	0.781	0.728	0.789	0.828	0.802	0.786	<u>0.831</u>
Credit	A-R	0.958	0.957	0.934	0.703	0.552	0.504	<u>0.957</u>	0.957	0.954	0.948	0.909	0.953	0.860	0.871	0.951
	R-A-R	<u>0.921</u>	0.919	0.882	0.535	0.379	0.483	0.919	0.918	0.914	0.902	0.843	0.914	0.809	0.784	0.904
	V-ROC	<u>0.917</u>	0.908	0.881	0.575	0.398	0.483	<u>0.914</u>	0.911	0.908	0.897	0.840	0.905	0.818	0.805	0.896
GECCO	A-R	0.970	0.952	0.795	0.714	0.516	0.555	<u>0.954</u>	0.949	0.947	0.936	0.769	0.804	0.619	0.711	0.557
	R-A-R	0.990	0.978	0.884	0.725	0.501	0.609	0.977	0.984	<u>0.987</u>	0.977	0.634	0.757	0.680	0.598	0.510
	V-ROC	<u>0.987</u>	0.975	0.871	0.717	0.503	0.593	0.974	0.979	<u>0.982</u>	0.971	0.637	0.756	0.677	0.595	0.503
Genesis	A-R	0.974	0.676	0.690	0.937	<u>0.947</u>	0.659	0.913	0.685	0.696	0.755	0.931	0.733	0.549	0.815	0.897
	R-A-R	0.981	0.727	0.797	0.975	<u>0.976</u>	0.744	0.919	0.737	0.741	0.791	0.917	0.734	0.693	0.822	0.819
	V-ROC	0.978	0.729	0.773	<u>0.971</u>	0.970	0.730	0.913	0.728	0.735	0.787	0.916	0.733	0.660	0.816	0.827
MSL	A-R	0.664	0.633	0.611	0.576	0.508	0.507	0.613	0.637	0.624	0.592	0.562	0.524	0.524	0.552	0.574
	R-A-R	0.747	0.708	0.686	0.662	0.529	0.596	0.701	<u>0.720</u>	0.703	0.681	0.635	0.594	0.575	0.631	0.643
	V-ROC	<u>0.735</u>	0.701	0.678	0.652	0.527	0.587	0.692	<u>0.712</u>	0.695	0.672	0.628	0.590	0.571	0.622	0.635
NYC	A-R	0.816	0.466	0.640	0.633	0.671	0.549	<u>0.791</u>	0.709	0.768	0.671	0.504	0.456	0.475	0.666	0.446
	R-A-R	0.836	0.598	0.697	0.754	0.753	0.524	<u>0.765</u>	0.722	0.762	0.706	0.636	0.612	0.632	0.744	0.545
	V-ROC	0.827	0.579	0.689	0.737	0.722	0.530	<u>0.771</u>	0.719	0.760	0.701	0.619	0.589	0.610	0.730	0.536
PSM	A-R	0.652	0.593	0.592	0.600	0.514	0.501	0.592	0.586	0.580	0.585	<u>0.650</u>	0.619	0.542	0.648	0.620
	R-A-R	0.640	0.588	0.589	0.507	0.453	0.489	<u>0.593</u>	0.586	0.579	0.585	0.587	0.530	0.543	0.584	0.572
	V-ROC	0.639	0.589	0.588	0.507	0.451	0.479	<u>0.593</u>	0.585	0.579	0.585	0.589	0.532	0.542	0.585	0.575
SMD	A-R	0.811	0.722	0.745	0.631	0.508	0.502	0.727	0.736	0.728	0.738	<u>0.774</u>	0.602	0.664	0.679	0.626
	R-A-R	0.800	0.743	0.762	0.594	0.500	0.505	0.747	0.760	0.754	0.762	<u>0.783</u>	0.579	0.679	0.656	0.597
	V-ROC	0.797	0.742	0.761	0.592	0.499	0.505	0.746	0.758	0.751	0.760	<u>0.782</u>	0.578	0.678	0.655	0.597
Contextual4.9	A-R	0.921	0.566	0.916	0.660	0.554	0.535	0.919	0.862	0.709	0.545	0.914	0.706	0.840	0.538	0.470
	R-A-R	0.859	0.386	0.851	0.504	0.396	0.405	<u>0.856</u>	0.761	0.543	0.391	0.848	0.517	0.736	0.364	0.310
	V-ROC	0.854	0.443	0.845	0.548	0.431	0.422	<u>0.850</u>	0.768	0.586	0.437	0.842	0.563	0.743	0.405	0.362
Contextual7.2	A-R	0.899	0.558	0.893	0.536	0.539	0.514	<u>0.897</u>	0.845	0.691	0.515	0.879	0.716	0.802	0.538	0.458
	R-A-R	0.818	0.388	0.812	0.361	0.374	0.436	<u>0.816</u>	0.730	0.522	0.360	0.789	0.530	0.674	0.362	0.297
	V-ROC	0.822	0.442	0.814	0.424	0.406	0.443	<u>0.819</u>	0.746	0.567	0.409	0.797	0.585	0.693	0.401	0.351
Global4.8	A-R	0.998	0.885	0.981	0.631	0.560	0.515	0.991	0.993	0.981	0.685	0.996	0.998	0.947	0.770	0.609
	R-A-R	<u>0.995</u>	0.804	0.963	0.464	0.388	0.383	0.982	0.986	0.962	0.554	<u>0.991</u>	0.916	0.654	0.454	
	V-ROC	0.979	0.806	0.952	0.533	0.430	0.402	0.967	0.967	0.942	0.579	0.972	<u>0.973</u>	0.903	0.687	0.489
Global7.2	A-R	0.997	0.861	0.971	0.559	0.568	0.513	0.988	0.992	0.978	0.665	<u>0.996</u>	0.995	0.928	0.745	0.608
	R-A-R	0.993	0.772	0.948	0.395	0.403	0.383	0.977	0.984	0.957	0.534	<u>0.992</u>	0.989	0.886	0.618	0.478
	V-ROC	0.979	0.772	0.937	0.442	0.397	0.397	0.962	0.966	0.939	0.560	<u>0.972</u>	0.970	0.878	0.653	0.512
Seasonal4.8	A-R	0.999	0.511	0.945	0.865	0.590	0.661	0.958	0.922	0.819	0.613	0.943	0.840	0.921	0.447	0.522
	R-A-R	1.000	0.613	0.929	<u>0.972</u>	0.560	0.642	0.933	0.932	0.847	0.676	0.895	0.849	0.898	0.573	0.629
	V-ROC	0.999	0.596	0.929	<u>0.950</u>	0.567	0.634	0.932	0.929	0.839	0.668	0.896	0.845	0.897	0.544	0.609
Seasonal7.7	A-R	0.997	0.513	0.946	0.537	0.579	0.628	<u>0.959</u>	0.921	0.827	0.634	0.954	0.817	0.915	0.426	0.509
	R-A-R	0.997	0.640	<u>0.946</u>	0.638	0.558	0.623	0.943	0.931	0.860	0.691	0.907	0.844	0.914	0.583	0.615
	V-ROC	0.994	0.615	0.945	0.616	0.559	0.611	<u>0.946</u>	0.929	0.851	0.680	0.915	0.838	0.913	0.546	0.602
Shapelet4.9	A-R	0.982	0.527	0.856	0.623	0.532	0.627	0.871	0.812	0.670	0.552	0.857	0.651	0.767	0.490	0.342
	R-A-R	0.996	0.608	<u>0.883</u>	0.742	0.608	0.602	0.880	0.851	0.714	0.642	0.854	0.716	0.800	0.624	0.510
	V-ROC	0.992	0.599	0.874	0.723	0.594	0.596	<u>0.875</u>	0.844	0.712	0.627	0.851	0.711	0.794	0.601	0.485
Shapelet7.4	A-R	0.957	0.518	0.872	0.523	0.506	0.567	<u>0.882</u>	0.824	0.697	0.573	0.874	0.660	0.728	0.545	0.332
	R-A-R	0.991	0.618	0.877	0.624	0.527	0.546	<u>0.885</u>	0.860	0.748	0.640	0.853	0.745	0.780	0.687	0.512
	V-ROC	0.984	0.606	0.876	0.603	0.518	0.537	<u>0.885</u>	0.853	0.741	0.633	0.856	0.727	0.771	0.658	0.486
Mixture5.7	A-R	0.906	0.628	0.859	0.524	0.490	0.577	0.870	0.850	0.692	0.648	0.452	0.440	<u>0.881</u>	0.470	0.443
	R-A-R	0.910	0.746	0.909	0.649	0.466	0.519	<u>0.910</u>	0.902	0.759	0.738	0.390	0.386	0.876	0.394	0.465
	V-ROC	0.900	0.726	0.899	0.623	0.463	0.522	<u>0.902</u>	0.892	0.745	0.722	0.385	0.381	0.877	0.389	0.458
Mixture5.9	A-R	0.879	0.596	0.834	0.523	0.509	0.562	0.845	0.819	0.650	0.636	0.513	0.503	<u>0.874</u>	0.497	0.492
	R-A-R	0.887	0.706	0.866	0.630	0.509	0.552	0.871	0.857	0.723	0.728	0.505	0.476	<u>0.878</u>	0.463	0.548
	V-ROC	0.880	0.687	0.860	0.610	0.501	0.542	0.865	0.850	0.708	0.710	0.490	0.462	<u>0.876</u>	0.446	0.531
Trend4.8	A-R	0.944	0.705	0.881	0.561	0.502	0.530	0.877	0.868	0.733	0.719	0.477	0.463	<u>0.943</u>	0.525	0.532
	R-A-R	0.956	0.876	0.920	0.620	0.502	0.503	0.924	0.929	0.						

1080
1081
1082
1083
1084
1085

Table 7: Average A-P (AUC-PR), R-A-P (R-AUC-PR) and V-PR (VUS-PR) accuracy measures for all datasets. The best results are highlighted in bold, and the second-best results are underlined.

Dataset	Metric	CATCH	Modern	iTrans	DuaITF	ATrans	DC	TsNet	Patch	DLin	NLin	AE	Ocsvm	IF	PCA	HBOS
CICIDS	A-P	0.002	0.001	0.002	0.002	0.001	0.002	0.002	0.001	0.002	0.001	0.001	0.001	0.003	0.001	0.003
	R-A-P	0.002	0.002	0.002	0.001	0.001	0.001	0.002	0.002	0.002	0.002	0.001	0.364	<u>0.002</u>	0.001	0.002
	V-PR	0.003	0.002	0.002	0.001	0.002	0.002	0.002	0.002	0.002	0.002	0.002	0.389	<u>0.003</u>	0.001	0.002
CallIt2	A-P	<u>0.114</u>	0.054	0.106	0.057	0.045	0.035	0.078	0.116	0.097	0.054	0.084	0.095	0.080	0.073	0.080
	R-A-P	<u>0.124</u>	0.070	0.111	0.088	0.089	0.087	0.092	<u>0.115</u>	0.097	0.073	0.096	0.109	0.095	0.106	0.113
	V-PR	<u>0.121</u>	0.070	0.110	0.082	0.083	0.083	0.090	<u>0.115</u>	0.095	0.072	0.097	0.109	0.091	0.103	0.108
Credit	A-P	<u>0.101</u>	0.088	0.042	0.023	0.007	0.002	0.091	0.089	0.081	0.087	0.040	0.053	0.074	0.029	0.173
	R-A-P	0.053	0.054	0.024	0.009	0.002	0.002	<u>0.056</u>	0.054	0.053	0.053	0.020	0.038	0.040	0.009	0.081
	V-PR	0.051	0.051	0.024	0.011	0.002	0.002	<u>0.053</u>	0.051	0.050	0.051	0.020	0.037	0.039	0.012	0.076
GECCO	A-P	<u>0.418</u>	0.447	0.096	0.130	0.013	0.012	0.410	0.400	0.349	0.304	0.206	0.039	0.052	0.234	0.199
	R-A-P	<u>0.473</u>	<u>0.459</u>	0.134	0.050	0.022	0.020	0.428	0.444	0.416	0.372	0.033	0.098	0.085	0.047	0.032
	V-PR	<u>0.465</u>	<u>0.461</u>	0.128	0.049	0.022	0.019	0.429	0.439	0.406	0.363	0.033	0.101	0.083	0.046	0.033
Genesis	A-P	0.249	0.015	0.019	0.051	0.058	0.010	0.036	0.013	0.017	0.011	0.055	0.007	0.005	0.011	0.059
	R-A-P	0.384	0.015	0.021	0.101	0.101	0.012	0.038	0.013	0.016	0.013	0.047	0.506	0.011	0.015	0.090
	V-PR	<u>0.371</u>	0.015	0.020	0.097	0.095	0.012	0.037	0.013	0.016	0.014	0.047	0.506	0.010	0.015	0.087
MSL	A-P	<u>0.167</u>	0.146	0.151	0.156	0.107	0.107	0.146	0.157	0.147	0.140	0.148	0.153	0.114	<u>0.157</u>	0.132
	R-A-P	<u>0.260</u>	0.224	0.227	0.220	0.165	0.157	0.231	<u>0.242</u>	0.225	0.222	0.200	0.185	0.174	0.203	0.190
	V-PR	<u>0.256</u>	0.220	0.224	0.218	0.162	0.156	0.227	<u>0.237</u>	0.221	0.218	0.199	0.185	0.173	0.200	0.189
NYC	A-P	<u>0.076</u>	0.020	0.033	0.040	0.045	0.034	0.060	0.046	0.046	<u>0.062</u>	0.025	0.020	0.022	0.046	0.019
	R-A-P	<u>0.120</u>	0.038	0.051	0.065	0.096	0.045	0.069	0.059	0.061	0.066	0.046	0.333	0.047	0.076	0.031
	V-PR	<u>0.114</u>	0.037	0.051	0.063	0.087	0.047	0.070	0.059	0.061	0.065	0.045	0.318	0.045	0.072	0.032
PSM	A-P	0.434	0.385	0.383	0.411	0.298	0.281	0.391	0.378	0.371	0.376	<u>0.465</u>	0.418	0.334	0.468	0.394
	R-A-P	<u>0.435</u>	0.383	0.386	0.353	0.293	0.283	0.395	0.379	0.372	0.378	0.420	0.369	0.334	<u>0.423</u>	0.369
	V-PR	<u>0.436</u>	0.384	0.387	0.354	0.293	0.283	0.395	0.380	0.373	0.379	0.420	0.370	0.334	<u>0.423</u>	0.370
SMD	A-P	<u>0.172</u>	0.130	0.146	0.069	0.046	0.043	0.141	0.147	0.139	0.141	0.188	0.104	0.122	0.128	0.145
	R-A-P	0.159	0.130	0.145	0.070	0.055	0.046	0.140	0.152	0.145	0.145	0.182	0.080	0.099	0.109	0.088
	V-PR	<u>0.159</u>	0.130	0.145	0.070	0.054	0.046	0.140	0.152	0.144	0.145	0.181	0.081	0.099	0.109	0.088
Contextual4.9	A-P	<u>0.754</u>	0.090	0.754	0.086	0.070	0.054	0.773	0.640	0.274	0.055	0.732	0.522	0.323	0.066	0.044
	R-A-P	0.585	0.060	<u>0.585</u>	0.075	0.055	0.055	0.614	0.432	0.135	0.054	0.556	0.293	0.225	0.054	0.047
	V-PR	<u>0.562</u>	0.074	0.559	0.094	0.068	0.067	0.586	0.423	0.148	0.066	0.534	0.292	0.230	0.068	0.057
Contextual7.2	A-P	0.770	0.106	0.756	0.087	0.099	0.074	<u>0.767</u>	0.672	0.309	0.090	0.721	0.542	0.374	0.105	0.075
	R-A-P	<u>0.612</u>	0.083	0.594	0.078	0.078	0.079	<u>0.608</u>	0.477	0.166	0.075	0.546	0.324	0.260	0.079	0.067
	V-PR	<u>0.594</u>	0.100	0.579	0.097	0.094	0.094	<u>0.590</u>	0.469	0.183	0.090	0.533	0.333	0.271	0.098	0.081
Global4.8	A-P	0.978	0.552	0.939	0.087	0.064	0.051	0.959	0.959	0.927	0.099	0.971	0.981	0.435	0.136	0.113
	R-A-P	<u>0.957</u>	0.363	0.881	0.068	0.055	0.050	0.918	0.918	0.858	0.077	0.942	0.961	0.404	0.110	0.063
	V-PR	<u>0.901</u>	0.361	0.834	0.092	0.069	0.062	0.866	0.864	0.808	0.089	0.884	0.903	0.394	0.140	0.074
Global7.2	A-P	0.974	0.517	0.921	0.088	0.098	0.074	0.947	0.960	0.912	0.134	0.973	0.977	0.492	0.182	0.106
	R-A-P	<u>0.949</u>	0.346	0.854	0.082	0.084	0.074	0.902	0.923	0.834	0.106	0.948	0.953	0.429	0.145	0.090
	V-PR	<u>0.905</u>	0.347	0.818	0.099	0.101	0.089	0.860	0.876	0.876	0.122	0.899	<u>0.904</u>	0.426	0.182	0.107
Seasonal4.8	A-P	<u>0.975</u>	0.055	0.865	0.476	0.158	0.128	<u>0.889</u>	0.776	0.622	0.063	0.884	0.732	0.727	0.061	0.058
	R-A-P	<u>0.994</u>	0.087	0.739	0.719	0.162	0.223	<u>0.750</u>	0.681	0.540	0.099	0.718	0.604	0.679	0.092	0.088
	V-PR	<u>0.987</u>	0.084	0.755	0.676	0.165	0.210	<u>0.763</u>	0.695	0.551	0.099	0.737	0.621	0.679	0.091	0.085
Seasonal7.7	A-P	0.963	0.092	0.881	0.083	0.164	0.148	<u>0.906</u>	0.773	0.645	0.109	0.900	0.734	0.733	0.116	0.080
	R-A-P	<u>0.978</u>	0.148	<u>0.808</u>	0.139	0.192	0.260	0.805	0.723	0.599	0.163	0.758	0.645	0.752	0.169	0.132
	V-PR	<u>0.963</u>	0.141	0.819	0.134	0.194	0.246	<u>0.823</u>	0.732	0.605	0.159	0.782	0.658	0.743	0.160	0.132
Shapelet4.9	A-P	0.774	0.087	0.651	0.089	0.109	0.133	0.708	0.542	0.449	0.089	<u>0.715</u>	0.537	0.295	0.136	0.062
	R-A-P	<u>0.921</u>	0.132	0.608	0.149	0.143	0.169	<u>0.639</u>	0.528	0.416	0.137	0.619	0.488	0.352	0.241	0.104
	V-PR	<u>0.877</u>	0.133	0.616	0.148	0.137	0.164	<u>0.653</u>	0.534	0.422	0.136	0.634	0.496	0.343	0.224	0.101
Mixture5.7	A-P	<u>0.368</u>	0.196	0.238	0.060	0.060	0.088	0.268	0.273	0.172	0.104	0.068	0.050	0.591	0.082	0.051
	R-A-P	<u>0.509</u>	0.276	0.349	0.110	0.092	0.146	0.363	0.369	0.204	0.160	0.091	0.125	0.579	0.092	0.122
	V-PR	<u>0.477</u>	0.264	0.339	0.106	0.090	0.143	0.352	0.357	0.233	0.236	0.162	0.246	0.577	0.090	0.125
Mixture5.9	A-P	0.355	0.182	0.311	0.091	0.091	0.133	<u>0.365</u>	0.298	0.197	0.167	0.128	0.090	0.593	0.090	0.089
	R-A-P	<u>0.490</u>	0.253	0.386	0.160	0.152	0.199	0.403	0.364	0.239	0.243	0.165	0.250	0.627	0.154	0.226
	V-PR	<u>0.468</u>	0.247	0.375	0.157	0.150	0.192	0.393	0.357	0.233	0.236	0.162	0.246	0.619	0.151	0.221
Trend4.8	A-P	<u>0.377</u>	0.215	0.254	0.062	0.048	0.063	0.274	0.228	0.155	0.133	0.056	0.044	0.615	0.054	0.054
	R-A-P	<u>0.538</u>	0.343	0.368	0.093	0.092	0.040	0.385	0.241	0.223	0.090	0.330	0.589	0.092	0.239	
	V-PR	<u>0.516</u>	0.329	0.360	0.092	0.097	0.092	0.389	0.375	0.237	0.216	0.089	0.318	0.588	0.091	0.233
Trend7.8	A-P	0.510	0.520	0.327	0.126	0.106	0.078	0.384	0.501	0.459	0.359	0.091	0.075	<u>0.511</u>	0.075	0.082
	R-A-P	<u>0.665</u>	0.514	0.399	0.173	0.171	0.128	0.435	0.521	0.429	0.391	0.154	0.261	<u>0.550</u>	0.135	0.250
	V-PR	<u>0.637</u>	0.515	0.386	0.169	0.166	0.125	0.424	0.512	0.429	0.389	0.1				

Table 8: Average Acc (Accuracy), P (Precision), R (Recall) and F1 (F1-score) accuracy measures for all datasets. The best results are highlighted in bold, and the second-best results are underlined.

	Dataset	Metric	CATCH	Modern	iTrans	DualTF	ATrans	DC	TsNet	Patch	DLin	NLin	AE	Ocsvm	IF	PCA	HBOS
CICIDS	Acc	0.758	0.750	0.762	0.565	0.745	0.750	0.750	0.751	0.757	0.754	0.994	0.082	0.852	0.656	0.913	
	P	0.003	0.001	0.002	0.001	0.001	0.001	0.001	0.001	<u>0.002</u>	0.001	0.000	0.001	0.000	0.001	0.000	
	R	<u>0.759</u>	0.278	0.481	0.595	0.253	0.266	0.354	0.380	0.506	0.380	0.000	0.987	0.063	0.405	0.013	
	F1	0.006	0.002	0.004	0.003	0.002	0.002	0.003	0.003	<u>0.004</u>	0.003	0.000	0.002	0.001	0.002	0.000	
CallIt2	Acc	0.946	0.889	0.930	0.910	0.944	0.841	0.946	0.889	0.887	0.844	<u>0.960</u>	0.867	0.968	0.884	0.886	
	P	0.138	0.074	0.124	0.073	0.085	0.034	0.104	0.091	0.083	0.066	0.067	0.089	<u>0.125</u>	0.084	0.075	
	R	0.162	0.243	0.230	0.176	0.095	0.162	0.108	0.311	0.284	<u>0.324</u>	0.027	0.378	0.014	0.297	0.257	
	F1	<u>0.149</u>	0.114	0.161	0.103	0.090	0.056	0.106	0.141	0.098	0.128	0.109	0.038	0.144	0.024	0.131	0.117
Credit	Acc	0.981	0.981	0.951	0.688	0.847	0.716	0.981	0.980	0.981	0.980	0.994	0.893	0.996	0.868	0.847	
	P	<u>0.059</u>	0.058	0.026	0.003	0.001	0.001	0.058	0.058	0.057	0.057	0.047	0.013	0.156	0.009	0.009	
	R	0.758	0.740	0.843	0.596	0.139	0.238	0.740	0.749	0.726	0.744	0.135	<u>0.901</u>	0.283	0.731	0.915	
	F1	<u>0.110</u>	0.107	0.051	0.006	0.003	0.003	0.107	0.107	0.105	0.107	0.069	0.026	0.201	0.017	0.018	
GECCO	Acc	0.984	0.984	0.981	0.612	0.983	0.979	0.984	<u>0.989</u>	0.981	0.987	0.888	0.055	0.989	0.240	0.590	
	P	0.380	0.373	0.173	0.009	0.012	0.008	0.379	0.475	0.332	<u>0.384</u>	0.021	0.011	0.214	0.014	0.014	
	R	0.818	0.779	0.207	0.340	0.008	0.008	0.804	0.585	0.781	0.460	0.215	0.993	0.012	0.988	0.542	
	F1	<u>0.518</u>	0.504	0.189	0.018	0.010	0.008	0.516	0.524	0.466	0.418	0.039	0.022	0.023	0.027	0.027	
Genesis	Acc	0.992	0.965	0.986	0.970	0.931	<u>0.991</u>	0.991	0.987	0.987	0.972	0.987	0.424	0.983	0.888	0.771	
	P	<u>0.116</u>	0.015	0.065	0.066	0.053	0.016	0.119	0.075	0.055	0.013	0.047	0.007	0.006	0.017	0.017	
	R	0.160	0.120	0.180	0.500	0.960	0.020	0.200	0.200	0.140	0.080	0.120	1.000	0.020	0.480	0.980	
	F1	<u>0.134</u>	0.027	0.095	0.116	0.100	0.018	0.149	0.109	0.079	0.022	0.068	0.014	0.009	0.033	0.033	
MSL	Acc	0.853	0.857	0.854	0.891	0.891	0.892	0.855	0.873	0.858	0.872	<u>0.891</u>	0.818	0.890	0.812	0.816	
	P	0.185	0.166	0.158	0.248	0.143	0.181	0.166	0.194	0.173	0.193	<u>0.219</u>	0.128	0.180	0.130	0.127	
	R	0.117	0.090	0.089	0.019	0.008	0.008	0.093	0.066	0.093	0.067	0.014	0.125	0.014	0.137	0.128	
	F1	0.143	0.117	0.114	0.035	0.015	0.016	0.119	0.098	0.121	0.100	0.026	0.126	0.025	<u>0.133</u>	0.127	
NYC	Acc	0.978	0.972	0.797	0.977	0.977	0.977	0.976	0.976	0.976	0.977	0.974	0.029	0.974	0.904	0.895	
	P	1.000	0.000	0.034	0.111	<u>0.333</u>	0.250	0.000	0.000	0.000	0.000	0.059	0.022	0.056	0.059	0.000	
	R	0.010	0.000	<u>0.293</u>	0.010	0.010	0.010	0.000	0.000	0.000	0.000	0.010	0.980	0.010	0.222	0.000	
	F1	0.020	0.000	<u>0.061</u>	0.019	0.020	0.019	0.000	0.000	0.000	0.000	0.017	0.043	0.017	0.094	0.000	
PSM	Acc	0.730	0.729	0.728	0.697	0.719	0.615	0.726	0.729	0.726	0.728	0.715	0.737	0.723	0.682	<u>0.736</u>	
	P	0.624	0.653	0.600	0.461	0.396	0.278	0.591	0.653	<u>0.658</u>	0.644	0.444	0.548	0.802	0.427	0.544	
	R	0.064	0.047	0.058	0.559	0.025	0.243	0.048	0.047	0.025	0.047	0.110	0.299	0.004	0.421	0.302	
	F1	0.116	0.089	0.105	0.506	0.046	0.259	0.088	0.088	0.047	0.087	0.176	0.387	0.007	<u>0.424</u>	0.389	
SMD	Acc	0.918	0.931	0.914	0.863	0.952	0.774	0.931	0.934	0.943	0.943	0.959	0.865	<u>0.958</u>	0.860	0.841	
	P	0.194	0.151	0.162	0.091	0.112	0.042	0.176	0.185	0.197	0.201	0.706	0.107	<u>0.454</u>	0.117	0.095	
	R	0.305	0.145	0.255	0.257	0.022	0.201	0.181	0.173	0.124	0.126	0.007	0.304	0.020	0.359	<u>0.332</u>	
	F1	0.237	0.148	<u>0.198</u>	0.135	0.037	0.069	0.178	0.179	0.152	0.155	0.014	0.158	0.039	0.176	0.148	
Contextual4.9	Acc	<u>0.961</u>	0.734	0.957	0.713	0.641	0.618	0.734	0.888	0.943	0.742	0.965	0.888	0.956	0.848	0.865	
	P	<u>0.584</u>	0.067	0.555	0.044	0.051	0.049	0.101	0.264	0.446	0.119	0.670	0.234	0.577	0.072	0.029	
	R	0.733	0.340	0.696	0.235	0.356	0.364	0.559	<u>0.713</u>	0.656	0.656	0.591	0.559	0.393	0.174	0.053	
	F1	0.650	0.112	0.618	0.075	0.089	0.086	0.172	0.385	0.531	0.201	<u>0.628</u>	0.330	0.467	0.102	0.037	
Contextual7.2	Acc	0.960	0.721	0.937	0.603	0.702	0.611	0.739	0.886	0.893	0.729	0.715	0.737	0.723	0.682	<u>0.736</u>	
	P	<u>0.744</u>	0.095	0.548	0.085	0.080	0.067	0.157	0.352	0.373	0.160	0.775	0.306	0.633	0.103	0.053	
	R	0.686	<u>0.336</u>	0.719	0.461	0.297	0.342	0.600	<u>0.700</u>	<u>0.717</u>	0.650	0.556	0.556	0.350	0.197	0.064	
	F1	0.714	0.148	0.622	0.143	0.126	0.112	0.249	0.468	0.491	0.257	<u>0.647</u>	0.394	0.451	0.135	0.058	
Global4.8	Acc	0.993	0.896	<u>0.994</u>	0.833	0.174	0.639	0.989	0.995	0.993	0.895	0.980	0.903	0.977	0.698	0.872	
	P	0.936	0.277	1.000	0.071	0.048	0.046	0.900	1.000	0.977	0.920	0.747	0.331	0.766	0.109	0.086	
	R	<u>0.921</u>	0.721	0.875	0.204	0.854	0.329	0.858	0.888	0.871	0.825	0.875	0.996	0.750	0.738	0.175	
	F1	0.929	0.400	<u>0.933</u>	0.105	0.090	0.080	0.878	0.940	0.921	0.429	0.806	0.496	0.758	0.190	0.116	
Global7.2	Acc	0.978	0.849	0.972	0.326	0.232	0.665	0.987	0.984	0.985	0.900	0.978	0.915	0.970	0.644	0.843	
	P	0.804	0.281	0.764	0.075	0.074	0.077	0.984	0.873	0.915	0.401	0.871	0.458	0.834	0.134	0.062	
	R	<u>0.925</u>	0.713	0.883	0.738	0.836	0.334	0.836	0.916	0.872	0.802	0.808	0.983	0.727	0.721	0.084	
	F1	0.860	0.403	0.819	0.136	0.135	0.125	0.904	<u>0.894</u>	0.893	0.534	0.838	0.625	0.777	0.226	0.071	
Seasonal4.8	Acc	0.988	0.861	0.973	0.956	0.956	0.952	<u>0.974</u>	0.974	0.974	0.964	0.959	0.890	0.957	0.855	0.863	
	P	0.994	0.065	1.000	0.653	0.889	0.531	<u>1.000</u>	1.000	1.000	0.984	0.630	0.269	0.610	0.062	0.043	
	R	0.747	0.141	0.444	0.195	0.100	0.071	0.461	0.456	0.461	0.253	0.361	<u>0.743</u>	0.311	0.141	0.087	
	F1	<u>0.853</u>	0.089	0.615	0.300	0.179	0.125	0.631	0.627	0.631	0.403	0.459	0.395	0.412	0.086	0.058	
Seasonal7.7	Acc	0.979	0.792	0.964	0.894	0.928	0.925	0.963	0.960	<u>0.965</u>	0.943	0.938	0.887	0.939	0.839	0.849	
	P	0.961	0.080	1.000	0.092	0.968	0.597	0.995	0.960	<u>1.000</u>	0.963	0.692	0.379	0.766	0.099	0.103	
	R	0.765	0.160	0.530	0.041	0.078	0.103	0.522	0.506	0.543	0.271	0.359	<u>0.726</u>	0.313	0.134	0.124	
	F1	0.852	0.107	0.693	0.057	0.144	0.176	0.685	0.664	0.704	0.423	0.473	0.498	0.444	0.114	0.113	
Shapelet4.9	Acc	0.969	0.820	0.966	0.942	0.950	0.946	0.967	0.953	<u>0.968</u>	0.94						

1188
 1189
 1190
 1191
 1192
 1193

Table 9: Average R-R (Range-Recall), R-P (Range-Precision) and R-F (Range-F1-score) accuracy measures for all datasets. The best results are highlighted in bold, and the second-best results are underlined.

1194
 1195
 1196

Dataset	Metric	CATCH	Modern	iTrans	DualTF	ATrans	DC	TsNet	Patch	DLin	NLin	AE	Ocsvm	IF	PCA	HBOS	
CICIDS	R-R	0.786	0.277	0.494	0.586	0.243	0.283	0.369	0.389	0.523	0.386	0.000	0.986	0.057	0.394	0.009	
	R-P	<u>0.004</u>	0.002	0.002	0.001	0.001	0.001	0.002	0.002	0.003	0.001	0.000	0.004	0.001	0.001	0.000	
	R-F	<u>0.007</u>	0.003	0.004	0.003	0.003	0.002	0.003	0.004	0.005	0.003	0.000	0.008	0.001	0.003	0.000	
CallIt2	R-R	0.278	0.318	0.344	0.209	0.161	0.205	0.161	0.424	0.315	0.325	0.055	<u>0.359</u>	0.031	0.280	0.309	
	R-P	0.139	0.069	0.113	0.056	0.105	0.031	0.095	0.077	0.091	0.064	0.067	<u>0.096</u>	<u>0.125</u>	0.099	0.086	
	R-F	0.185	0.114	<u>0.170</u>	0.088	0.127	0.053	0.120	0.131	0.142	0.107	0.060	0.152	0.049	0.147	0.134	
Credit	R-R	0.735	0.716	0.828	0.564	0.150	0.234	0.716	0.275	0.701	0.721	0.135	<u>0.892</u>	0.292	0.709	0.907	
	R-P	<u>0.054</u>	0.052	0.024	0.002	0.003	0.002	0.051	0.052	0.049	0.052	0.047	0.012	0.156	0.008	0.009	
	R-F	<u>0.101</u>	0.097	0.047	0.004	0.007	0.003	0.096	0.096	0.092	0.097	0.070	0.023	0.204	0.015	0.017	
GECCO	R-R	0.795	0.644	0.266	0.146	0.063	0.040	0.782	0.366	0.790	0.274	0.188	<u>0.953</u>	0.030	0.986	0.361	
	R-P	0.065	0.086	0.111	0.039	0.013	0.008	0.053	0.289	0.042	0.296	0.021	0.006	0.214	0.041	0.016	
	R-F	0.119	0.152	0.156	0.062	0.022	0.013	0.099	0.323	0.080	<u>0.285</u>	0.038	0.011	0.052	0.079	0.031	
Genesis	R-R	0.497	0.174	0.507	0.550	0.855	0.079	0.211	0.385	0.180	0.162	0.356	1.000	0.077	0.325	0.861	
	R-P	0.119	0.014	0.057	0.030	0.005	0.016	<u>0.086</u>	0.067	0.059	0.013	0.047	0.003	0.006	0.035	0.002	
	R-F	<u>0.192</u>	0.026	0.102	0.058	0.010	0.027	<u>0.122</u>	0.114	0.089	0.024	0.083	0.005	0.011	0.063	0.005	
MSL	R-R	0.241	0.194	0.182	0.049	0.150	0.126	0.224	0.176	0.202	0.162	0.110	0.202	0.112	0.237	0.199	
	R-P	0.150	0.129	0.125	0.267	0.143	0.179	0.130	0.136	0.130	0.137	<u>0.219</u>	0.098	0.180	0.113	0.119	
	R-F	0.185	0.155	0.148	0.084	0.146	0.148	<u>0.164</u>	0.153	0.158	0.149	0.146	0.132	0.138	0.153	0.149	
NYC	R-R	0.208	0.000	0.223	0.208	0.208	0.208	0.000	0.000	0.000	0.000	0.208	0.461	0.208	0.289	0.000	
	R-P	1.000	0.000	0.023	0.143	<u>0.333</u>	0.250	0.000	0.000	0.000	0.000	0.059	0.040	0.056	0.053	0.000	
	R-F	<u>0.344</u>	0.000	0.042	0.169	<u>0.256</u>	0.227	0.000	0.000	0.000	0.000	0.092	0.074	0.088	0.000	0.000	
PSM	R-R	0.450	0.376	<u>0.470</u>	0.410	0.133	0.211	0.455	0.370	0.399	0.359	0.230	0.133	0.139	0.505	0.265	
	R-P	0.557	0.553	0.533	0.456	0.374	0.274	0.537	0.557	0.584	<u>0.587</u>	0.444	0.385	0.802	0.459	0.467	
	R-F	<u>0.498</u>	0.448	0.499	0.432	0.197	0.238	0.493	0.444	0.474	0.446	0.303	0.198	0.237	0.481	0.338	
SMD	R-R	0.478	0.378	0.360	0.187	0.126	0.276	0.385	<u>0.426</u>	0.400	0.384	0.079	0.323	0.122	0.404	0.297	
	R-P	0.095	0.092	0.115	0.055	0.101	0.042	0.110	0.121	0.124	0.131	0.706	0.067	<u>0.454</u>	0.123	0.062	
	R-F	0.158	0.148	0.175	0.085	0.112	0.073	0.171	0.189	0.189	0.196	0.143	0.111	<u>0.192</u>	0.188	0.103	
Contextual4.9	R-R	0.733	0.341	0.697	0.232	0.347	0.361	0.556	<u>0.709</u>	0.656	0.659	0.603	0.559	0.396	0.181	0.053	
	R-P	<u>0.586</u>	0.071	0.559	0.041	0.057	0.047	0.139	0.267	0.440	0.125	0.670	0.240	0.577	0.061	0.025	
	R-F	0.651	0.118	0.620	0.069	0.097	0.083	0.222	0.388	0.526	0.210	<u>0.635</u>	0.336	0.470	0.092	0.034	
Contextual7.2	R-R	0.692	0.335	0.725	0.453	0.291	0.345	0.597	0.697	0.717	0.654	0.580	0.553	0.360	0.192	0.061	
	R-P	<u>0.744</u>	0.100	0.546	0.070	0.080	0.060	0.227	0.353	0.365	0.164	0.775	0.304	0.633	0.087	0.053	
	R-F	<u>0.717</u>	0.154	0.623	0.122	0.125	0.103	0.328	0.468	0.483	0.263	<u>0.664</u>	0.392	0.459	0.120	0.057	
Global4.8	R-R	<u>0.919</u>	0.726	0.874	0.206	0.859	0.327	0.855	0.887	0.870	0.823	0.887	0.996	0.759	0.733	0.178	
	R-P	0.939	0.292	1.000	0.073	0.041	0.043	0.900	<u>1.000</u>	0.978	0.362	0.747	0.338	0.766	0.113	0.116	
	R-F	0.929	0.416	<u>0.933</u>	0.108	0.079	0.076	0.877	0.940	0.921	0.503	0.811	0.505	0.762	0.196	0.140	
Global7.2	R-R	<u>0.922</u>	0.716	0.881	0.742	0.840	0.320	0.832	0.916	0.869	0.801	0.849	0.982	0.761	0.712	0.083	
	R-P	0.832	0.297	0.773	0.078	0.052	0.072	0.984	0.874	0.917	0.460	0.871	0.457	0.834	0.125	0.070	
	R-F	0.874	0.420	0.824	0.141	0.097	0.117	0.902	0.894	0.892	0.584	0.860	0.624	0.796	0.213	0.076	
Seasonal4.8	R-R	0.475	0.244	0.464	0.247	0.238	0.170	0.453	0.441	0.433	0.364	0.280	0.478	0.280	0.238	0.187	
	R-P	0.999	0.062	1.000	0.597	0.864	0.500	<u>1.000</u>	1.000	1.000	0.966	0.630	0.113	0.610	0.065	0.041	
	R-F	0.644	0.099	<u>0.634</u>	0.350	0.373	0.254	0.624	0.612	0.604	0.529	0.387	0.182	0.383	0.102	0.067	
Seasonal7.7	R-R	0.480	0.254	0.425	0.089	0.173	0.191	0.423	0.409	0.397	0.355	0.278	<u>0.453</u>	0.278	0.187	0.223	
	R-P	0.944	0.071	1.000	0.112	0.962	0.588	0.993	0.917	<u>1.000</u>	0.926	0.692	0.178	0.766	0.063	0.149	
	R-F	0.636	0.111	<u>0.596</u>	0.099	0.293	0.289	0.594	0.566	0.569	0.513	0.396	0.256	0.408	0.094	0.179	
Shapelet4.9	R-R	<u>0.447</u>	0.297	0.431	0.057	0.154	0.174	0.398	0.445	0.445	0.249	0.279	0.496	0.244	0.224	0.116	
	R-P	<u>0.944</u>	0.065	0.679	0.104	0.433	0.382	0.964	0.348	0.778	0.479	0.598	0.083	0.542	0.057	0.036	
	R-F	0.607	0.107	0.527	0.074	0.227	0.240	0.564	0.391	<u>0.566</u>	0.230	0.353	0.143	0.336	0.091	0.055	
Shapelet7.4	R-R	0.471	0.304	<u>0.473</u>	0.197	0.138	0.343	0.343	0.442	0.457	0.466	0.365	0.277	0.517	0.253	0.315	0.096
	R-P	0.980	0.083	0.620	0.123	0.309	0.153	<u>0.818</u>	0.479	0.598	0.211	0.583	0.118	0.489	0.114	0.042	
	R-F	0.636	0.130	0.536	0.151	0.191	0.212	<u>0.574</u>	0.468	0.524	0.268	0.375	0.193	0.333	0.168	0.058	
Mixture5.7	R-R	0.601	0.341	0.508	0.347	0.076	0.119	0.515	0.487	0.705	0.364	0.279	<u>0.954</u>	0.279	0.954	0.718	
	R-P	0.455	0.091	0.355	0.062	0.100	0.333	<u>0.509</u>	0.344	0.666	0.233	0.066	0.053	0.542	0.057	0.036	
	R-F	0.518	0.143	0.418	0.106	0.086	0.175	<u>0.512</u>	0.403	0.121	0.284	0.107	0.100	0.386	0.165	0.170	
Mixture5.9	R-R	0.670	0.293	0.595	0.343	0.057	0.145	0.599	0.558	0.594	0.465	0.279	<u>0.998</u>	0.267	1.000	0.806	
	R-P	<u>0.516</u>	0.148	0.401	0.089	0.070	0.443	0.511	0.342	0.108	0.217	0.092	0.000	0.704	0.000	0.116	
	R-F	0.583	0.197	0.479	0.141	0.063	0.218	<u>0.551</u>	0.424	0.183	0.296	0.139	0.000	0.387	0.000	0.203	
Trend4.8	R-R	0.910	0.492	0.562	0.277	0.023	0.082	0.474	0.483	0.625	0.538	0.280	<u>0.997</u>	0.268	1.000	0.799	
	R-P	0.247	0.157	0.205	0.073	0.037	0.167	<u>0.273</u>	0.169	0.064	0.117	0.048	0.000	0.600	0.002	0.050	
	R-F	0.388	0.238	0.300	0.115	0.029	0.110	0.347									

Table 10: Average Aff-P (Affiliated-Precision), Aff-R (Affiliated-Recall) and Aff-F (Affiliated-F1-score) accuracy measures for all datasets. The best results are highlighted in bold, and the second-best results are underlined.

Dataset	Metric	CATCH	Modern	iTrans	DualTF	ATrans	DC	TsNet	Patch	DLin	NLin	AE	Ocsvm	IF	PCA	HBOS
CICIDS	Aff-P	0.667	0.563	<u>0.586</u>	0.553	0.531	0.533	0.566	0.569	0.575	0.579	0.543	0.530	0.548	0.541	0.538
	Aff-R	<u>0.959</u>	0.781	0.892	0.926	0.593	0.882	0.783	0.785	0.799	0.794	0.156	1.000	0.672	0.724	0.545
	Aff-F	0.787	0.654	<u>0.708</u>	0.692	0.560	0.664	0.657	0.660	0.669	0.669	0.243	0.693	0.604	0.619	0.542
CallIt2	Aff-P	0.742	0.650	<u>0.703</u>	0.617	0.645	0.571	0.691	0.667	0.668	0.616	0.560	0.652	0.539	0.688	0.620
	Aff-R	0.955	0.975	0.963	0.959	0.838	0.894	0.932	0.976	0.976	0.984	0.617	<u>0.982</u>	0.321	0.869	0.969
	Aff-F	0.835	0.780	<u>0.812</u>	0.751	0.729	0.697	0.794	0.793	0.793	0.757	0.587	0.783	0.402	0.768	0.756
Credit	Aff-P	<u>0.618</u>	0.611	0.559	0.513	0.521	0.488	0.610	0.612	0.605	0.608	0.560	0.556	0.658	0.564	0.533
	Aff-R	0.956	0.952	0.984	0.935	0.865	0.898	0.953	0.955	0.948	0.952	0.562	<u>0.997</u>	0.612	0.959	0.999
	Aff-F	0.750	0.744	0.713	0.663	0.650	0.632	0.744	<u>0.746</u>	0.738	0.742	0.561	0.714	0.634	0.710	0.695
GECCO	Aff-P	<u>0.832</u>	0.808	0.735	0.633	0.690	0.567	0.810	0.831	0.808	0.793	0.836	0.499	0.647	0.646	0.620
	Aff-R	0.998	0.998	0.979	0.786	0.903	0.872	0.997	0.995	0.997	0.992	0.810	1.000	0.315	<u>1.000</u>	0.827
	Aff-F	0.908	0.893	0.839	0.701	0.782	0.687	0.894	<u>0.906</u>	0.893	0.882	0.823	0.666	0.424	0.785	0.708
Genesis	Aff-P	0.835	0.728	<u>0.822</u>	0.683	0.749	0.659	0.780	0.763	0.772	0.724	0.759	0.512	0.673	0.691	0.564
	Aff-R	0.966	0.974	0.972	0.996	1.000	0.943	0.968	0.974	0.959	0.971	0.976	1.000	0.951	0.991	<u>1.000</u>
	Aff-F	0.896	0.833	<u>0.891</u>	0.810	0.856	0.776	0.864	0.856	0.856	0.829	0.854	0.677	0.788	0.814	0.721
MSL	Aff-P	0.599	0.578	0.566	0.562	0.549	0.576	<u>0.589</u>	0.584	0.577	0.584	0.521	0.497	0.502	0.538	0.520
	Aff-R	0.966	0.975	0.951	0.618	0.933	0.874	0.973	0.952	<u>0.975</u>	0.948	0.781	0.902	0.697	0.914	0.982
	Aff-F	0.740	0.726	0.710	0.588	0.692	0.694	<u>0.734</u>	0.724	0.725	0.723	0.625	0.641	0.584	0.678	0.680
NYC	Aff-P	1.000	0.639	0.520	0.551	0.751	0.769	0.750	0.719	0.814	<u>0.817</u>	0.529	0.500	0.481	0.516	0.525
	Aff-R	0.989	<u>0.965</u>	0.999	0.988	0.988	0.980	0.843	0.843	0.843	0.821	0.989	1.000	0.989	0.997	0.946
	Aff-F	0.994	0.769	0.684	0.708	0.853	<u>0.862</u>	0.794	0.776	0.828	0.819	0.689	0.667	0.648	0.680	0.675
PSM	Aff-P	<u>0.808</u>	0.734	0.765	0.622	0.600	0.538	0.762	0.739	0.777	0.762	0.776	0.652	0.904	0.712	0.621
	Aff-R	0.918	0.941	0.966	0.868	0.871	0.932	0.939	<u>0.948</u>	0.893	0.942	0.649	0.447	0.472	0.692	0.700
	Aff-F	0.859	0.825	<u>0.854</u>	0.725	0.710	0.682	0.842	0.831	0.843	0.707	0.531	0.620	0.702	0.658	
SMD	Aff-P	0.773	0.755	0.736	0.527	0.607	0.510	0.745	0.748	0.761	0.762	0.889	0.649	<u>0.801</u>	0.680	0.557
	Aff-R	0.938	0.948	0.943	0.956	0.895	0.998	0.938	0.970	0.940	0.946	0.291	0.866	0.513	0.807	0.722
	Aff-F	0.847	0.840	0.827	0.679	0.724	0.675	0.831	<u>0.845</u>	0.841	0.844	0.439	0.742	0.626	0.738	0.629
Contextual4.9	Aff-P	0.838	0.505	0.821	0.503	0.517	0.490	0.552	0.669	0.773	0.563	<u>0.861</u>	0.619	0.861	0.488	0.487
	Aff-R	0.812	0.814	0.761	0.776	0.792	0.779	0.837	<u>0.883</u>	0.806	0.908	0.674	0.769	0.582	0.463	0.547
	Aff-F	0.825	0.623	<u>0.790</u>	0.611	0.625	0.602	0.666	0.761	0.789	0.695	0.756	0.686	0.694	0.475	0.515
Contextual7.2	Aff-P	0.907	0.508	0.826	0.519	0.498	0.496	0.566	0.705	0.709	0.585	0.901	0.660	0.877	0.505	0.476
	Aff-R	0.748	0.782	0.803	0.905	0.685	0.735	0.806	0.851	0.841	<u>0.887</u>	0.647	0.760	0.535	0.447	0.422
	Aff-F	0.820	0.616	<u>0.814</u>	0.660	0.577	0.592	0.665	0.771	0.770	0.705	0.753	0.707	0.665	0.474	0.447
Global4.8	Aff-P	0.985	0.661	1.000	0.549	0.506	0.479	0.964	1.000	0.994	0.971	0.916	0.713	0.938	0.599	0.535
	Aff-R	0.922	0.867	0.876	0.749	<u>0.933</u>	0.737	0.865	0.889	0.875	0.907	0.912	0.996	0.900	0.894	0.554
	Aff-F	0.953	0.750	0.934	0.633	0.656	0.581	0.912	<u>0.941</u>	0.930	0.804	0.914	0.831	0.919	0.717	0.544
Global7.2	Aff-P	0.954	0.662	0.926	0.515	0.506	0.481	0.993	0.949	<u>0.975</u>	0.769	0.958	0.771	0.950	0.572	0.514
	Aff-R	0.935	0.857	0.893	<u>0.939</u>	0.937	0.648	0.836	0.928	0.881	0.861	0.895	0.993	0.866	0.872	0.510
	Aff-F	0.945	0.746	0.909	0.665	0.657	0.552	0.907	<u>0.938</u>	0.926	0.812	0.925	0.868	0.906	0.691	0.512
Seasonal4.8	Aff-P	1.000	0.533	1.000	0.950	0.945	0.912	<u>1.000</u>	1.000	1.000	0.993	0.970	0.654	0.859	0.534	0.509
	Aff-R	0.998	0.955	0.986	0.761	0.784	0.847	0.987	0.987	0.988	0.931	0.994	<u>0.998</u>	0.993	0.893	0.944
	Aff-F	0.999	0.684	0.993	0.845	0.857	0.879	0.993	0.994	<u>0.994</u>	0.961	0.928	0.790	0.921	0.668	
Seasonal7.7	Aff-P	0.992	0.534	1.000	0.628	0.970	0.882	0.998	0.985	<u>1.000</u>	0.982	0.868	0.697	0.925	0.482	0.546
	Aff-R	0.998	0.934	0.983	0.809	0.570	0.800	0.982	0.983	0.986	0.901	<u>0.994</u>	0.988	0.817	0.919	
	Aff-F	0.995	0.679	0.992	0.707	0.718	0.839	0.990	0.984	<u>0.993</u>	0.940	0.925	0.820	0.956	0.606	0.685
Shapelet4.9	Aff-P	0.997	0.517	0.952	0.653	0.779	0.763	0.968	0.874	<u>0.979</u>	0.646	0.732	0.606	0.832	0.547	0.492
	Aff-R	0.977	0.976	0.979	0.732	0.704	0.743	0.871	0.983	0.979	<u>0.987</u>	0.992	<u>0.988</u>	0.965	0.898	0.940
	Aff-F	0.987	0.676	0.966	0.690	0.740	0.753	0.917	0.925	<u>0.979</u>	0.744	0.842	0.751	0.894	0.680	0.646
Shapelet7.4	Aff-P	0.999	0.514	0.941	0.591	0.658	0.641	<u>0.965</u>	0.913	0.914	0.656	0.827	0.662	0.821	0.567	0.499
	Aff-R	0.969	0.975	0.972	0.842	0.659	0.823	0.967	0.970	0.974	0.930	0.943	0.985	0.983	0.949	0.873
	Aff-F	0.983	0.673	0.957	0.695	0.658	0.721	<u>0.966</u>	0.940	0.943	0.774	0.899	0.791	0.880	0.686	0.635
Mixture5.7	Aff-P	0.863	0.628	0.867	0.555	0.541	0.802	<u>0.875</u>	0.867	0.581	0.779	0.560	0.539	0.879	0.543	0.501
	Aff-R	0.991	0.940	0.920	0.910	0.721	0.737	0.920	0.922	0.959	0.927	0.992	0.998	0.970	0.997	0.969
	Aff-F	0.923	0.753	0.893	0.689	0.618	0.768	0.897	0.894	0.723	0.833	0.716	0.700	<u>0.922</u>	0.703	0.660
Mixture5.9	Aff-P	0.841	0.607	0.838	0.510	0.502	0.814	0.820	0.797	0.568	0.744	0.520	0.517	0.868	0.518	0.515
	Aff-R	0.988	0.871	0.991	0.954	0.608	0.820	0.989	0.990	0.975	0.927	0.991	0.929	0.991	1.000	0.947
	Aff-F	0.909	0.716	<u>0.908</u>	0.665	0.550	0.763	0.897	0.883	0.718	0.827	0.682	0.682	0.906	0.683	0.678
Trend4.8	Aff-P	0.861	0.812	0.831	0.505	0.560	0.751	0.861	0.840	0.571	0.765	0.502	0.502	0.877	0.505	0.503
	Aff-R	0.997	0.974	0.984	0.937	0.746	0.803	0.929	0.978	0.991	0.994	0.995	1.000	0.942	1.000	0.996
	Aff-F	0.924	0.886	0.901	0.656	0.640	0.776	0.893	0.904	0.724	0.865	0.667	0.668	<u>0.909</u>	0.671	0.668
T																

1296 Table 11: Average A-R (AUC-ROC) and Aff-F (Affiliated-F1) accuracy measures for 4 synthetic
 1297 datasets of different types of anomalies. The best results are highlighted in bold, and the second-
 1298 best results are underlined.
 1299

Model	CATCH		Modern		iTrans		DualTF		TFAD		
	Metric	Aff-F	A-R	Aff-F	A-R	Aff-F	A-R	Aff-F	A-R	Aff-F	A-R
Low-frequency anomalies		0.998	0.996	0.811	0.873	<u>0.850</u>	<u>0.929</u>	0.744	0.662	0.700	0.538
Mid-frequency anomalies		0.927	0.987	0.814	0.859	<u>0.913</u>	<u>0.984</u>	0.723	0.575	0.638	0.519
High-frequency anomalies		0.915	0.987	0.738	0.809	<u>0.864</u>	<u>0.927</u>	0.462	0.602	0.668	0.513
Not distinctly frequency band		0.873	0.917	0.775	0.765	<u>0.852</u>	<u>0.910</u>	0.720	0.630	0.619	0.495

D EMPIRICAL VERIFICATION SHOWS THAT CATCH CAN PERFORM FINE-GRAINED MODELING IN EACH FREQUENCY BAND

We design a set of experiments to validate the advantages of our method in capturing fine-grained frequency characteristics. We use the synthetic dataset creation method provided by TODS (Lai et al., 2021) to generate four synthetic datasets—see Figure 7, simulating scenarios with known frequency-specific anomalies: low-frequency anomalies, medium-frequency anomalies, high-frequency anomalies, and anomalies that are not distinctly separated across different frequency bands. We then test CATCH and several state-of-the-art methods on these datasets.

The experimental results in Table 11 show that CATCH consistently outperforms other algorithms across all four datasets. Notably, most algorithms perform poorly when dealing with time series containing high-frequency anomalies, while CATCH demonstrates outstanding performance. Furthermore, even on datasets where anomalies are distributed across multiple frequency bands with low separability, CATCH still achieves excellent results. These findings provide strong evidence that CATCH excels in capturing fine-grained frequency characteristics, significantly enhancing the performance of time series anomaly detection.

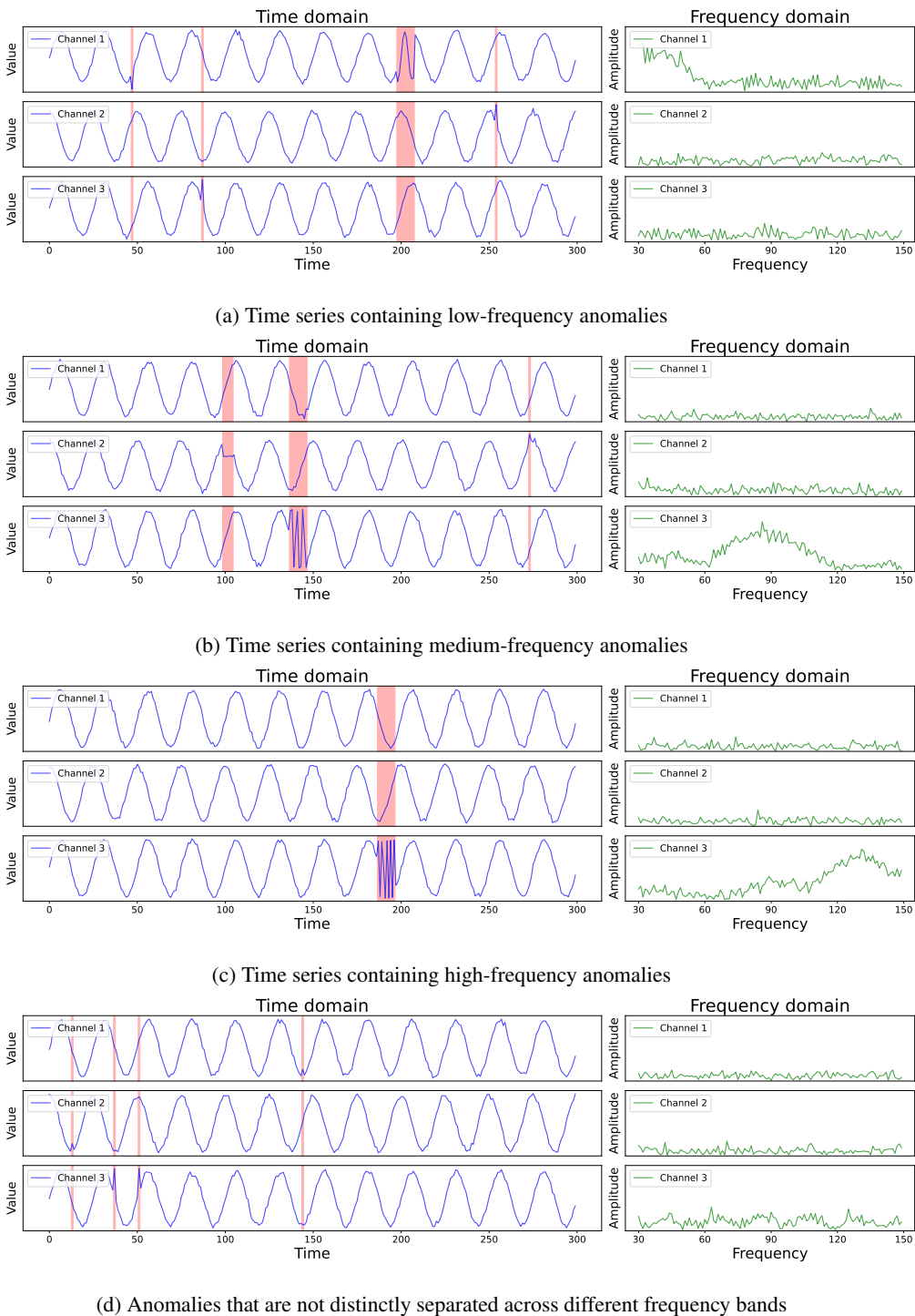


Figure 7: Four synthetic time series simulating scenarios with known frequency-specific anomalies.